Research Square

Preprints are preliminary reports that have not undergone peer review.
They should not be considered conclusive, used to inform clinical practice,
or referenced by the media as validated information.

Dual-action gum-based hydrogels: a ‘detect and detox’ platform for heavy metals in urine

Srishti Jagota
Manav Rachna University
Arpit Sand
sand.arpit@gmail.com

Manav Rachna University
Sudhir G Warkar
Delhi Technological University

Research Article

Keywords:

Posted Date: June 17th, 2026

DOI: https://doi.org/10.21203/rs.3.rs-9798032/v1

License: This work is licensed under a Creative Commons Attribution 4.0 International License.
Read Full License

Additional Declarations: No competing interests reported.

Dual-action gum-based hydrogels: a 'detect and detox' platform for heavy metals in urine

Srishti Jagota[1, 2], Arpit Sand[1*], Sudhir G Warkar[3]

[1]*Department of Science (Chemistry), Manav Rachna University, Faridabad - 121004 Haryana, India*

sand.arpit@mru.edu.in

[2]*Department of Forensic Science, Lloyd Institute of Forensic Science, Greater Noida, UP - 201310, India*

[3]*Delhi Technological University, Delhi, India 110042*

Abstract

In this study, we discuss the synthesis and characterization of a new type of Hydrogel Composite - a Dual Functional Hydrogel Composite - which was created to serve dual purposes: both for Colorimetric Detection of Heavy Metals in Urine, as well as Adsorption of Heavy Metals from Urine.

To create the Hydrogel Matrix we used Carboxymethyl Tamarind Kernel Gum (CMTKG), Guar Gum (GG) and Acrylamide (AAm), with the cross-linkers being combination of N, N'-Methylene bisacrylamide (MBA), initiator being Potassium per-sulfate (KPS) and accelerator is Tetramethylethylenediamine (TEMED). In addition, we incorporated Dithizone (DTZ) into the Hydrogel Composite to act as a Colorimetric Ligand to enable Naked-eye Detection.

The resulting transparent Hydrogel films had a high efficiency in DTZ loading, and so we evaluated the response of the Hydrogel Films to the toxic Metals Cadmium (Cd), Lead (Pb), Chromium (Cr), Nickel (Ni), Copper (Cu), Iron(Fe) and Mercury (Hg). The results of this study illustrate that the Hydrogel Composite functions well as a Colorimetric Sensor due to the well-documented ability of Hydrogel Composites to bind metals and the large color difference of heavy metal colorimetric and heavy metal Adsorption. The research presented here identifies a Novel Hydrogel Composite as a Low-Cost platform for Point-of-Care Heavy Metal Urine Detection, as well as Environmental Remediation.

Introduction

Heavy metals, such as cadmium (Cd), lead (Pb), chromium (Cr), nickel (Ni), copper (Cu), Iron (Fe) and mercury (Hg), cause threats to environmental safety and community health since they contaminate water resources and fluids in the body [1]. These metals accumulate in living organisms over a period of time and cause severe diseases, damage to organs, and neurological problems. Even though humans are exposed to these toxic metals primarily through contaminated food, water, and industrial waste, urine is one of the major routes for detecting bioaccumulation by monitoring biomarker levels [2].

Conventional detection techniques for heavy metals include atomic absorption spectroscopy and inductively coupled plasma-mass spectrometry. These two techniques present very sensitive and specific outcomes, but they are rather expensive, time-consuming, and require space in a central laboratory [3].

The low cost, ease of use, and visible interpretation make colorimetric sensors a possible alternative in helping solve some of these issues. Dithizone (DTZ) is one of the most used chromogenic agents because it forms a strong complex with heavy metals, hence changing color [4]. However, in most instances, DTZ in aqueous or biological solutions is difficult to use due to its low solubility, light sensitivity, and inability to recover/reuse [5]. Hydrogel-based immobilization systems use hydrogels made of naturally occurring polymeric compounds, such as Carboxymethyl Tamarind Kernel Gum or Guar Gum. Such hydrogels offer excellent biocompatibility, biodegradability, and functional versatility [6]. This study will report a newly developed, multifunctional hydrogel composite that incorporates CMTKG, GG, and AAm and cross-links by MBA, and also possesses redox-initiators systems. By further functionalizing with DTZ, the hydrogel allows colorimetric detection of metals, besides adsorptive removal. This method not only provides an easily visible and easy access on how to use equipment to perform such types of detection but also helps in the environmental remediation through sequestration of toxic ions.

The purpose of this research is to develop an inexpensive, portable, and environmentally friendly technique for rapid screening of urinary heavy metals, which would be very helpful in the future, especially in point-of-care diagnostic testing and the purification.

Comparative Analysis and State-of-the-Art (SOTA) Materials

To properly situate this work within the current state-of-the-art for heavy metal monitoring, it is essential to compare the conceptual and technical features of our platform with existing modalities. Traditional analytical methods, such as Inductively Coupled Plasma Mass Spectrometry (ICP-MS) and Atomic Absorption Spectroscopy (AAS), provide superior sensitivity but are fundamentally limited by high operational costs, sophisticated laboratory infrastructure, and an inability to perform in-situ, real-time testing.
To overcome these barriers, recent developments have shifted toward nanomaterial-based and polymeric colorimetric sensors. Table 1 summarizes how our dual-action platform compares with recent state-of-the-art materials in the literature.

TABLE 1: Comparative matrix of SOTA heavy metal sensing and remediation systems.

Material Matrix	Active Ligand / Agent	Detection Mechanism	Functionality	Limitations	Target Medium	Ref
TiO_2/poly(t-butyl acrylate-acrylic acid)	Dithizone (DTZ)	Colorimetric (Visual)	Detection Only	Lacks direct bulk adsorption/remediation capacity	Aqueous media	[66]
Carbon Nanofibers (CNFs)	Dithizone (DTZ)	Micro extraction / Analytical	Separation Only	Requires instrumentation; no naked-eye readout	Non-alcoholic beverages	[67]
Synthetic Polyacrylamide Hydrogels	Organic Chromophores	Optical Shift	Detection Only	Non-biodegradable; poor biocompatibility for bio-fluids	Waste water	[72]
Chitosan/Alginate Beads	Grafted Chelators	Adsorption Only	Remediation Only	No built-in visual signaling mechanism	Industrial effluent	[73]
DNAzyme-Functionalized Hydrogel	Catalytic DNA / Gold Nanoparticles	Colorimetric Optical Shift	Point-of-care diagnostics	High production cost; delicate enzyme stability; no remediation	Human Serum & Blood	[74]
Graphene Oxide/Chitosan Microbeads	Grafted Polyethylenimine	Surface Adsorption Chelation	Remediation / Sorption only	No built-in diagnostic or visual signaling mechanism	Industrial wastewater	[75]
Fluorescent Carbon Dots / Cellulose Matrix	Organic Fluorophore	Fluorometric Quenching (I/I_0)	Quantitative sensing only	High bio fluid auto fluorescence interference; no extraction	Human Blood & Urine	[76]
CMTKG/GG/AAm Hydrogel Composite (This Work)	Dithizone (DTZ)	Naked-eye Colorimetric + Chelation Adsorption	Dual-Action (‘Detect and Detox’)	Dependent on diffusion kinetics within the polymer mesh	Urinalysis & Aqueous Medium	Current Study

Conceptual and Technical Novelty of This Work

Unlike single-function platforms that either isolate sensing from environmental remediation or rely on toxic, non-biodegradable synthetic matrices, this study introduces a distinct **Dual-Action 'Detect and Detox' platform**. The structural and technical advances of this design reside in three key areas:

1. **Synergistic Sustainable Matrix:** By grafting Carboxymethyl Tamarind Kernel Gum (CMTKG) and Guar Gum (GG) with Acrylamide, we leverage an abundance of carboxyl (-COO^-) and hydroxyl (-OH) groups. This composition maximizes the hydrogel's water-retaining networks (achieving an equilibrium swelling capacity up to 1220%) and promotes rapid mass transfer of metal ions from complex biological fluids like urine.
2. **Immobilization without Leaching:** Free Dithizone (DTZ) is notoriously limited by poor water solubility and severe light sensitivity. Our platform achieves high-efficiency physical entrapment within a stabilized 3D porous network. This successfully suppresses DTZ leaching and degradation while retaining full accessibility to its metal-chelating sites.
3. **Simultaneous Chromogenic Signaling and Sequestration:** The hydrogel does not merely capture ions; it undergoes distinct, metal-specific visual color shifts (e.g., violet-pink for Hg^{2+}, greenish for Cu^{2+} at highly sensitive limits of visual detection (0.1 ppm). This allows the platform to function simultaneously as an immediate point-of-care screening tool and a structural matrix for heavy metal detoxification.

Experimental Section

Synthesis of the CMTKG/Guar Gum/Acrylamide Hydrogel Film

The Hydrogel membrane is fabricated through the free radical polymerization method of Carboxymethyl Tamarind Kernel Gum (CMTKG) and Guar Gum (GG) as the Biopolymers using Acrylamide (AAm) as a monomer and N,N'-methylenebisacrylamide (MBA) as the cross-linker and KPS and TEMED as redox initiators to begin the polymerization (Fig. 1).

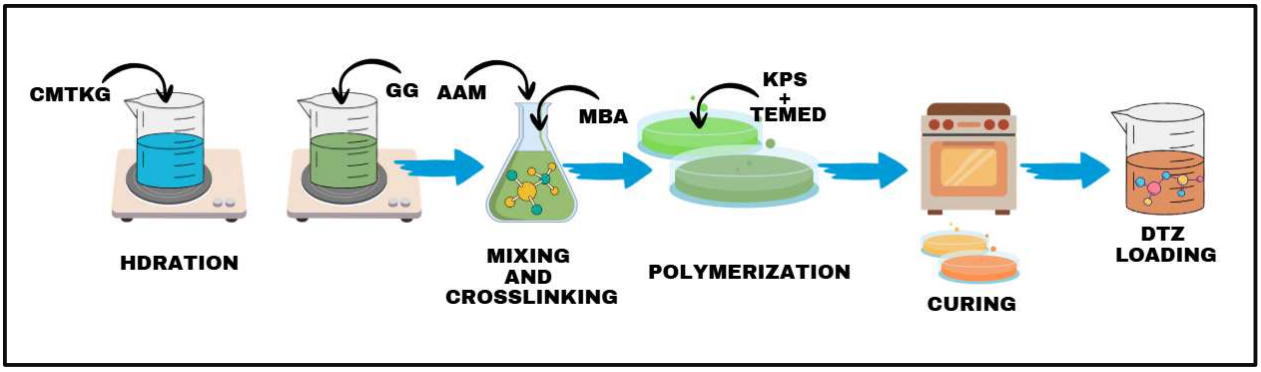


Fig. 1 Schematic representation of the synthesis process of the CMTKG-GG-PAM hydrogel.

First, 0.5g of CMTKG was added to 40ml of deionized water at a slow rate using a magnetic stirrer for 1.5 hours until it was fully hydrated and resulted in a clear solution. The same procedure of dissolving the 0.5g of GG in 40ml of deionized water was performed using magnetic stirring for 1.5 hours so that it was fully hydrated. The two viscous solutions were mixed thoroughly so that there was a homogenous dispersion of the two polysaccharides. 3g of AAm was then added to this mixture and mixed for another 15–20 minutes until it was dissolved.

Once all of the AAm was dissolved, 0.02g of MBA was added and mixed for another 30 minutes to ensure uniform distribution within the solution. To initiate the polymerization process, 0.045g of KPS was added followed by adding 0.01ml of TEMED and mixed at a slow rate to prevent the formation of bubbles. This initial solution was poured on a clean and level Petri dish and placed in the hot air oven at 65 degrees Celsius for 2–3 hours for complete polymerization and film formation.

Functionalization of the CMTKG/Guar Gum/Acrylamide Hydrogel Film

The first step for producing colorimetric-sensory hydrogel films is solvation using ethyl alcohol as a solvent (in a 2.5 mg/ml concentration) containing Dithizone (DTZ). Therefore, after curing the hydrogel films, they were cut into rectangular pieces and subsequently soaked in a 2.5 mg/ml ethanol solution of DTZ for 2 hours, shielded from light to avoid degradation during the process.

For removing debris, the films soaked in DTZ were thoroughly rinsed multiple times with deionized water until the wash water was clear, thus demonstrating that all unbounded DTZ was removed from the film and there was no residual DTZ in the films. After completion of this rinsing process, the resulting hydrogel film containing colorimetric sensory characteristics was stored in a cool dry dark location until further use.

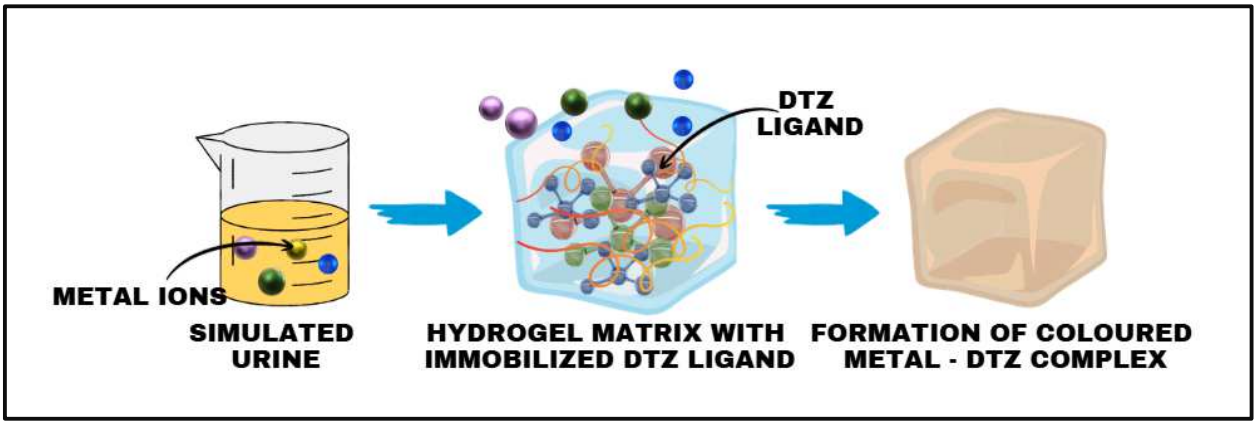


Fig. 2 Schematic illustration of the chelation-based colorimetric sensing mechanism for heavy metal detection using the DTZ-functionalized hydrogel.

To evaluate the performance of the resulting hydrogel films, both the visual colour change and adsorption efficiency were observed by conducting immersion tests in a 0.5 ppm concentration of artificial urine containing heavy metals (Fig. 2).

Swelling studies

Free Absorbency Capacity

The tea bag method was used to determine the absorbency of the prepared polymers. A tea bag containing an accurately weighed powdered sample (0.2±0.02 g) was immersed entirely in 200 ml of aqueous saline solution (0.9 wt. % of NaCl) and allowed to soak for 30 min at room temperature to reach equilibrium [7]. The tea bag was hung up for 15 minutes to remove excess fluid. The equilibrated absorbency (Qeq) was calculated using the following equation (1):

$$Qeq = \frac{W_{TB,f} - W_{TB,i}}{W_H} \quad (1)$$

Where W_H is the weight of the prepared polymer, $W_{TB,\,f}$ and $W_{TB,\,i}$ are the weights of the tea bag after and before water uptake, respectively. Five measurements were taken to give the average value.

Swelling behavior under various conditions

Over the course of 24 hours, the swelling behavior of the produced hydrogels was evaluated in pH 7.4 and 1.2 buffers. After precisely weighing the dried hydrogel (W_d), it was submerged in the appropriate solutions [8].
The hydrogel was removed, weighed (WS), and then re-immersed in the solution after one hour. The given equation (2) was used to measure swelling, which was done in triplicate.

$$Equilibrium\ Swelling\ (\%) = \frac{(W_s - W_d)}{W_d}\ x\ 100 \tag{2}$$

The swelling experiment in distilled water at temperatures ranging from 10 ◦C and 60 ◦C was used to evaluate the SAP's thermal responsiveness. Temperature control was achieved by using a water bath set to desired temperatures (above 25 degrees Celsius) and a refrigerator for temperatures below 25 degrees.

Gel Fraction

The weighted hydrogel (Wi) was immersed in distilled water for 24 hours, removed, dried in an oven at 60°C, and then weighed (We) once again in order to determine the gel fraction (cross linked portion) of produced hydrogels [9]. The following equation (3) was used to determine the gel fraction (%).

$$Gel\ Fraction\ (\%) = \frac{W_e}{W_i}\ x\ 100 \tag{3}$$

Porosity

Hexane was used as the solvent to assess the porosity of the produced hydrogels. For two hours, the dry hydrogel (Mi) was submerged in 10ml of hexane. The final weight (Mf) was noted upon the hydrogel's removal from the hexane [10]. The following formula (4) was used to determine the hydrogel's porosity:

$$Porosity\ (\%) = \frac{(W_f - W_i)}{\rho V}\ x\ 100 \tag{4}$$

Here, ρ and V stand for the hydrogel's volume and hexane's density (0.659 g/mL).

Sensing Studies

The colorimetric sensing behavior of the DTZ-functionalized hydrogel film was systematically investigated at different concentrations of metals and at different temperature ranges. For the concentration studies, artificial urine solutions were artificially contaminated with standard heavy metal ions (Cd^{2+}, Pb^{2+}, Cr^{3+}, Ni^{2+}, Cu^{2+}, Fe^{2+}, Hg^{2+}) at concentrations of 0.1 - 0.5 ppm. Hydrogel films of a uniform size were immersed in the same solutions for the same duration and color changes were photographed and recorded. For quantitative analysis, a UV-Vis spectrophotometer was used to measure the absorbance shift at specific wavelengths associated with the metal-DTZ complexes. The temperature sensitivity of the sensing mechanism was studied in a similar manner, using the same protocol (i.e.,

color changes of the films and solutions were photographed) over the temperature range of 5 - 60 °C. The test temperatures were equilibrated with the solutions and hydrogel films before immersing in them, and the following parameters were measured to evaluate the impact of temperature on the sensing mechanism and hydrogel performance: Color transition time, color intensity and color stability.

Results and Discussion

Synthesis and Macroscopic Properties

Using the free-radical technique of copolymerization, we were able to combine the Carboxymethyl tamarind kernel gum (CMTKG), guar gum (GG) and acrylamide (AAm) with N,N′-methylenebisacrylamide (MBA) as a cross-linking agent and KPS–TEMED as a redox initiator system at a polymerization temperature of 65°C for two to three hours (Fig. 4). The film produced from this process exhibited excellent mechanical properties such as transparency, flexibility, and stability (Fig. 3).


(a)

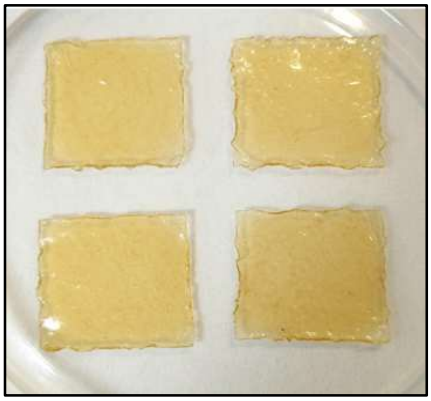
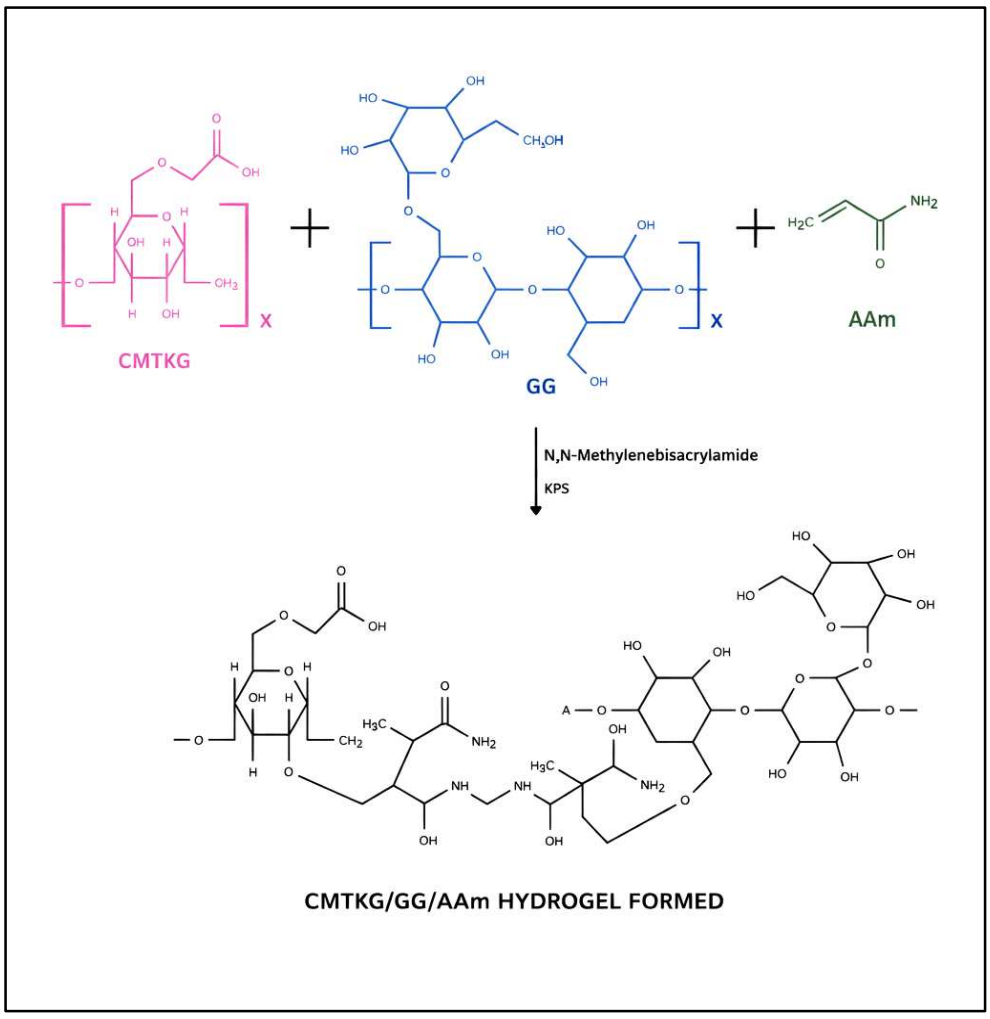

(b)

Fig. 3 (a) Formation of transparent CMTKG-GG-PAM polymer film (b) Successful incorporation of Dithizone in the hydrogel film


CMTKG
GG
AAm
N,N-Methylenebisacrylamide
KPS
CMTKG/GG/AAm HYDROGEL FORMED

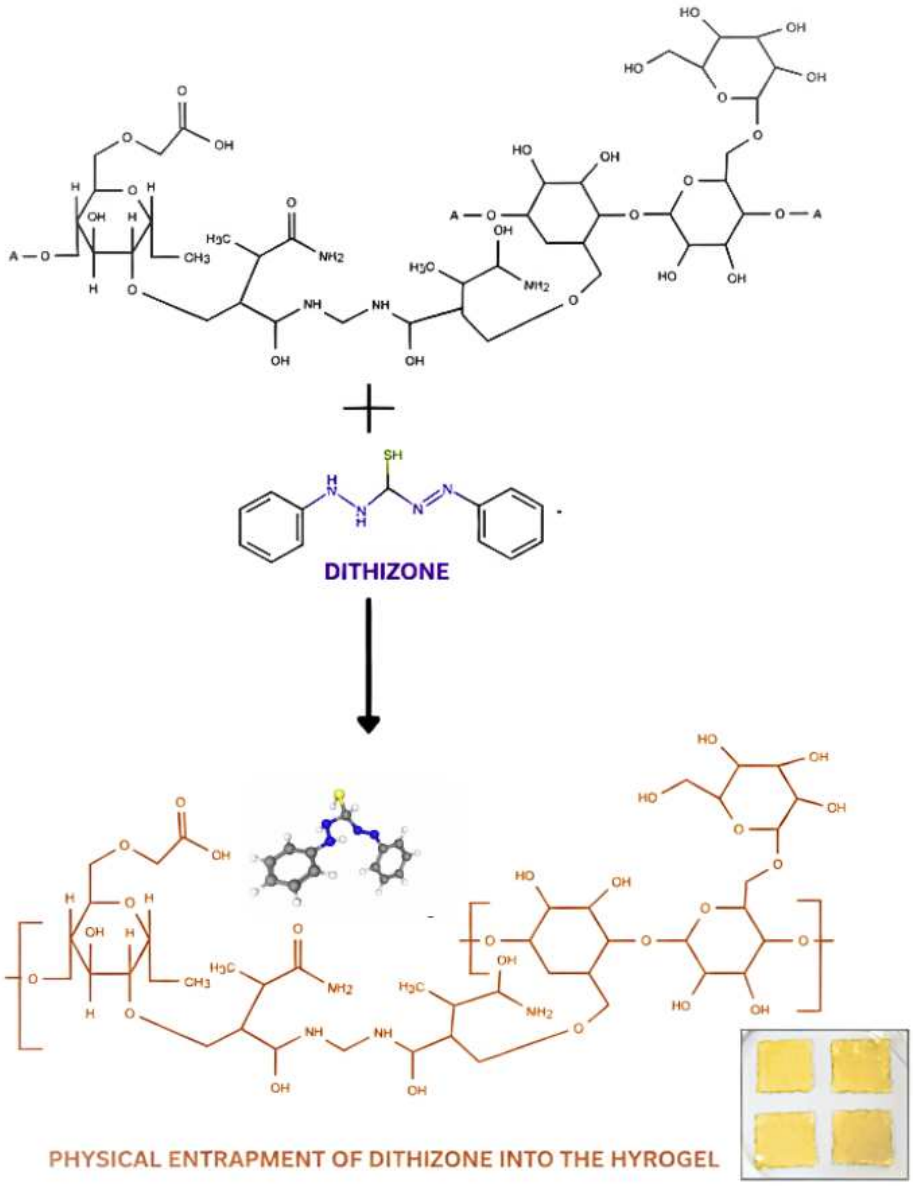


Fig. 4 Proposed chemical reaction mechanism and physical entrapment process for the hydrogel fabrication. **(a)** Synthesis of the CMTKG/GG/AAm hydrogel via free-radical graft copolymerization. **(b)** Schematic of the physical entrapment of Dithizone into the three-dimensional polymeric network.

When treated with dithizone (DTZ) by soaking in an ethanol solution, a pale orange color was uniformly seen throughout the entire film showing evidence of successful incorporation of the chromogenic ligand. The film maintained its shape during exposure to both aqueous and simulated urine environments; there was also no expected DTZ leaching or film dissolution when stored at room temperature. In summary, this indicates that the films will likely serve well as stable immobilization materials for use in sensor applications.

Sensory Analysis and Colorimetric Response

The DTZ-loaded CMTKG/guar gum/acrylamide hydrogel films showed intense and reproducible colorimetric responses to various metal ions, which clearly indicates that DTZ had been successfully immobilized within the polymeric matrix with retention of its metal-chelating property (Fig. 5). A different metal ion led to a different visual result due to DTZ–metal complexation: darkening with Fe^{2+}, greenish hue with Cu^{2+}, light peach and yellow colors with Pb^{2+} and Cd^{2+}, respectively, lighter coloration with both Ni^{2+} and Cr, and violet–pink color due to the Hg^{2+} ion (Fig. 6).

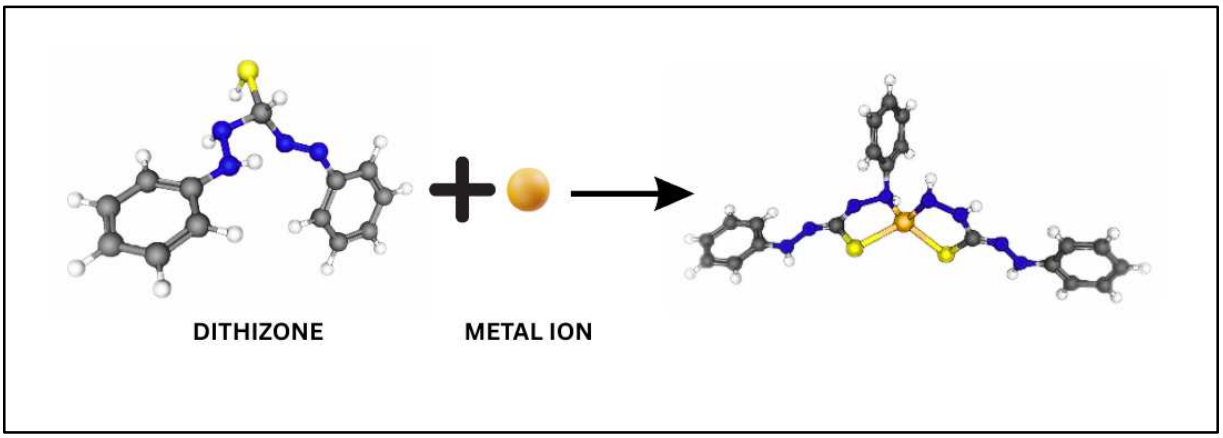


Fig. 5 Molecular modeling of the chelation reaction between the Dithizone (DTZ) ligand and a target metal ion.

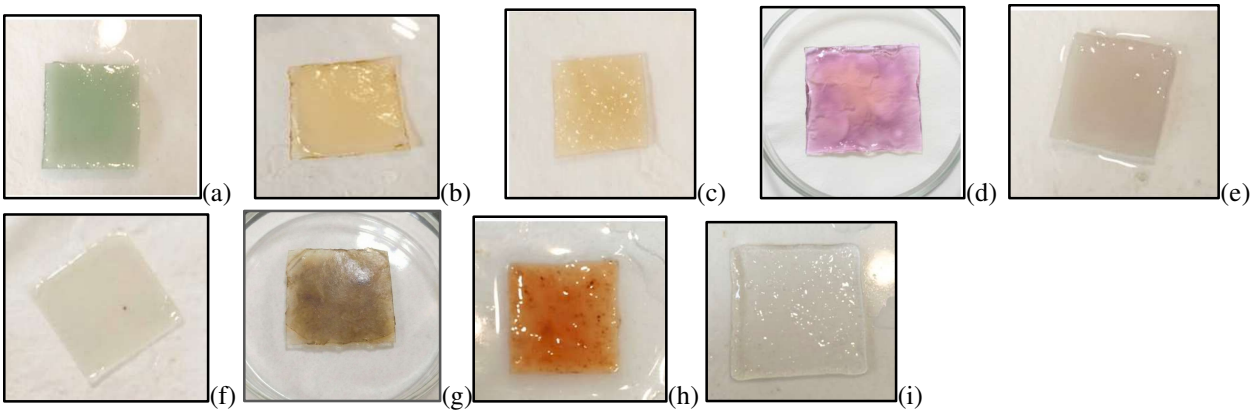


Fig. 6 Photographic evidence of the selective colorimetric response of the DTZ-functionalized hydrogel films toward various metal ions. (a) Cu^{2+} (b) Cd^{2+} (c) Pb^{2+} (d) Hg^{2+} (e) Cr^{2+} (f) Ni^{2+} (g) Fe^{2+} (h) DTZ - Control (i)Control without DTZ

The metal-free blank film containing DTZ preserved the original orange coloration of DTZ. On the other hand, a blank hydrogel without DTZ remained completely colorless, thus proving that the chromogenic response shown by the DTZ-loaded hydrogel film was purely due to the DTZ–metal interaction and not due to any polymer–metal interaction.

Swelling studies

Effect of pH

The swelling behavior of the CMTKG/GG/AAm hydrogel largely depends on the pH value of the surrounding medium. This is a function of the ionization states that the functional groups within this hydrogel find themselves. In highly acidic environments at pH 1.2, the swelling is greatly reduced at about 380% .This is because the carboxylate ($-COO^-$) groups on the CMTKG are largely protonated to the undissociated carboxylic acid (-COOH) form. This suppresses electrostatic repulsions among the polymer chains and thus favors the formation of intra- and intermolecular hydrogen bonds that result in a compact network that is contracted with little volume available for water to penetrate [11].

When the pH increases to a mildly acidic and neutral range, pH 4.0 to 7.0, swelling increases sharply, from 495% to 1220% (Fig. 7). This is due to progressive deprotonation of -COOH groups to form negatively charged $-COO^-$ anions [12]. The mutual electrostatic repulsion between these anionic sites forces the polymer chains to expand into larger pores and a more open network structure. At neutral pH (7.0), this "electrostatic repulsion" effect, together with the osmotic driving force from the hydrogel, gives maximum water absorption [13].

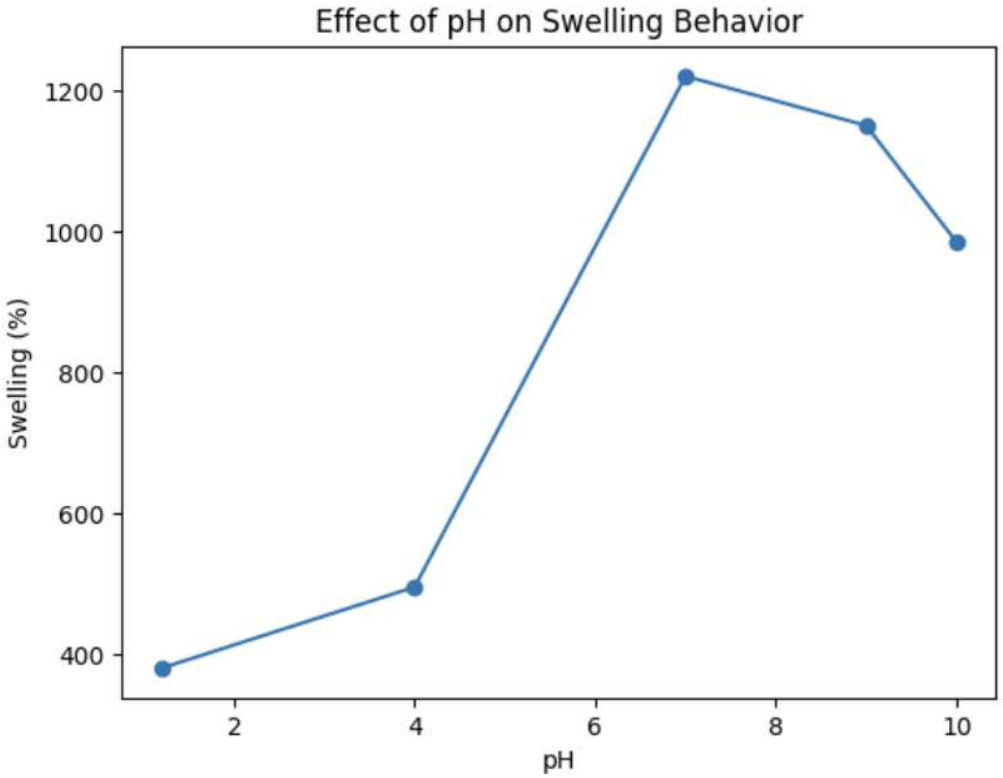


Fig. 7 Effect of pH variation on the equilibrium swelling behavior of the CMTKG-GG-PAM hydrogel.

At pH 9.0 and 10.0, a slight swelling decrease from the neutral maximum, from 1150% to 985%, is observed. While the polymer chains remain fully ionized at this increased pH, the high concentration of counter ions Na^+ in the surrounding medium acts to screen the negative charges borne by the polymer backbone [14]. This charge-screening effect lowers the intensity of electrostatic repulsion, partially collapsing the expanded network [15]. Besides this, the increased ionic strength of the solution diminishes the osmotic pressure difference between the interior of the hydrogel and the external medium-the major driving force for swelling-and, therefore, moderates the overall capacity for water uptake [16].

Effect of CMTKG

The CMTKG content governs the swelling capacity of the hydrogel directly through its hydrophilic and ionic character [17]. The swelling is poor (850%) at a lower concentration, for instance, with 0.3 g CMTKG, due to insufficient carboxylate -COO^- groups, which restrict both the osmotic driving force and electrostatic repulsion within the network [18]. When the content increases to an optimum, for example, 0.5 g, swelling increases to a maximum value of 1220% (Fig. 8), which is attributed to the ideal balance of hydrophilic sites and crosslinking density [19].

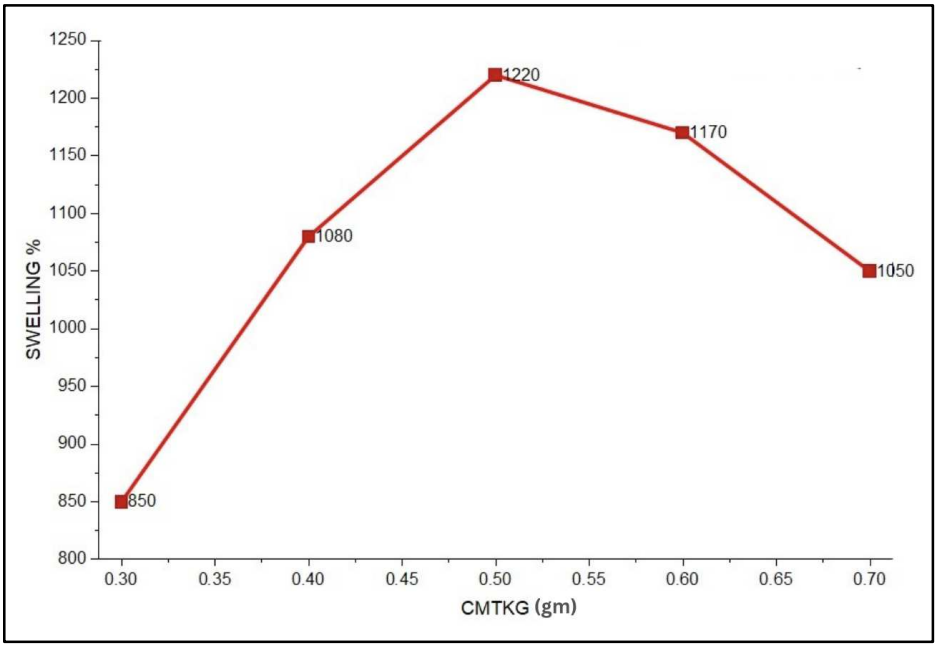


Fig. 8 Effect of CMTKG on the equilibrium swelling behavior of the CMTKG-GG-PAM hydrogel.

The high density of ionizable -COO^- groups enhances water uptake due to the Donnan equilibrium and chain expansion [20]. In contrast, beyond the optimum concentration (0.6-0.7 g), swelling decreases from 1170% to 1050% (Table 2)with increased polymer content, due to the increased viscosity during synthesis, which may affect homogeneous cross-linking and decrease the free volume for water uptake, despite the presence of more hydrophilic groups [21].

TABLE 2 Effect of CMTKG on the equilibrium swelling behavior of the CMTKG-GG-PAM hydrogel

Sample	**CMTKG**	**GG**	**AAm**	**MBA**	**KPS**	**Swelling percent**	**Gel Fraction**	**Porosity**
A1	0.3	0.5	3	0.02	0.045	850	85	50.5
A2	0.4	0.5	3	0.02	0.045	1080	88.2	54.8
A3	**0.5**	**0.5**	**3**	**0.02**	**0.045**	**1220**	**91.5**	**58.2**
A4	0.6	0.5	3	0.02	0.045	1170	90.0	56.5
A5	0.7	0.5	3	0.02	0.045	1050	87.5	52.0

Effect of GG

Guar gum is a galactomannan polysaccharide, and its main role in the swelling capacity of hydrogel is primarily due to its hydrophilic hydroxyl (-OH) groups. At low amounts, such as 0.3 g GG (Fig. 9), swelling is slight (approximately 920%) because there is insufficient hydrophilicity, resulting in limited interaction with the surrounding water [22].

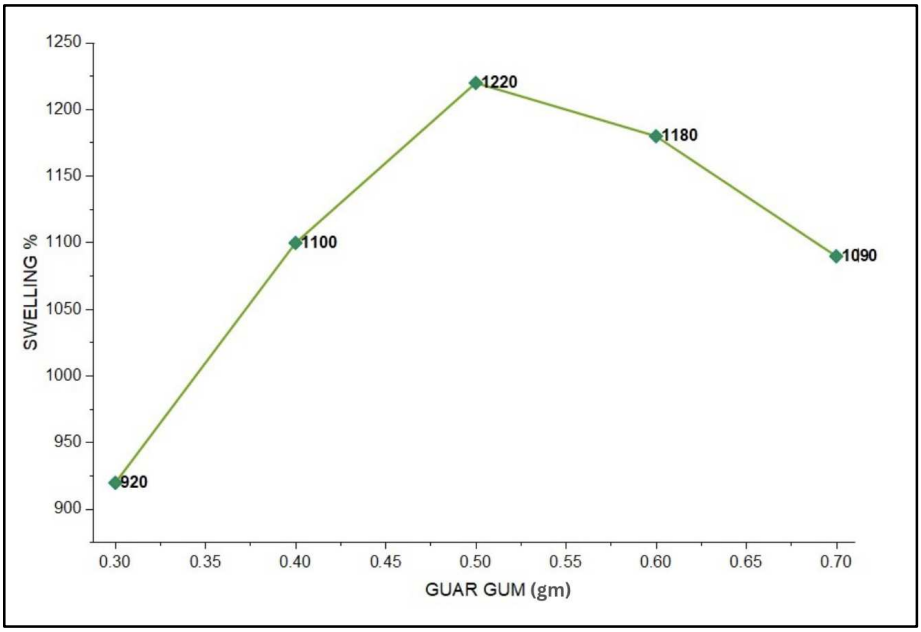


Fig. 9 Effect of Guar Gum on the equilibrium swelling behavior of the CMTKG-GG-PAM hydrogel

By increasing guar gum to an optimum value of about 0.5 g, swelling reaches a maximum of approximately 1220%. This takes place because an optimum value exists between the ability of guar gum to hold water and the structure of the overall crosslinked network, which together enhance water absorption and retention through hydrogen bonding and some flexible chain movement [23]. When further increased beyond this, up to 0.6–0.7 g, swelling decreases again to about 1180%–1090% (Table 3). This decrease arises because of the increased viscosity and chain entanglement that may hinder the further expansion of the network, decreasing the free space available for water diffusion inside it, although more hydrophilic sites are available [24].

TABLE 3 Effect of Guar Gum on the equilibrium swelling behavior of the CMTKG-GG-PAM hydrogel.

Sample	CMTKG	GG	AAm	MBA	KPS	Swelling percent	Gel Fraction	Porosity
A6	0.5	0.3	3	0.02	0.045	920	86	51
A7	0.5	0.4	3	0.02	0.045	1100	89	55.2
A8	**0.5**	**0.5**	**3**	**0.02**	**0.045**	**1220**	**91.5**	**58.2**
A9	0.5	0.6	3	0.02	0.045	1180	90.2	56

A10	0.5	0.7	3	0.02	0.045	1090	88	53.5

Effect of Acrylamide

Acrylamide is the key molecule forming the hydrogel network, causing the swelling because of its water-loving properties from the amide group (-$CONH_2$). A smaller amount, around 2.0 g of acrylamide, results in the gel swelling to only 980% (Fig. 10) , because there are fewer chains to provide the sites for water to be attracted to, causing the swelling [25]. Increasing the mass of acrylamide to the optimum level of 3.0 g, the swelling increases to the highest level, approximately 1220% [26].

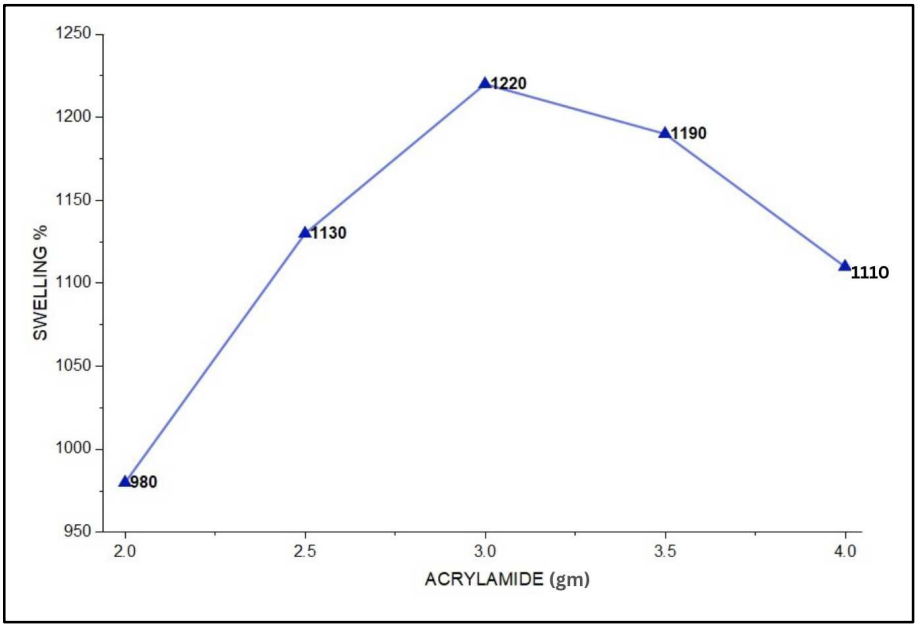


Fig. 10 Effect of Acrylamide on the equilibrium swelling behavior of the CMTKG-GG-PAM hydrogel.

Now the chains are at the optimal length and concentration, the hydrophilic sites are easily accessible for the addition of water by the process of hydrogen bonding, and the three-dimensional structure also holds the entire network while absorbing the water. Further increasing the concentration to above the optimum level, around 3.5-4.0 g, the swelling reduces to around 1190% to 1110% (Table 4). Now the chains have homo-polymerized to high extents, causing the chains to be unable to move freely, as there is also less free space to hold the water [27].

TABLE 4 Effect of Acrylamide on the equilibrium swelling behavior of the CMTKG-GG-PAM hydrogel.

Sample	**CMTKG**	**GG**	**AAm**	**MBA**	**KPS**	**Swelling percent**	**Gel Fraction**	**Porosity**
A11	0.5	0.5	2	0.02	0.045	980	88	52
A12	0.5	0.5	2.5	0.02	0.045	1130	90	55.5
A13	**0.5**	**0.5**	**3**	**0.02**	**0.045**	**1220**	**91.5**	**58.2**

A14	0.5	0.5	3.5	0.02	0.045	1190	90.8	57
A15	0.5	0.5	4	0.02	0.045	1110	89	54

Effect of MBA

N, N'-Methylenebisacrylamide, or MBA, is the key chemical cross-linker, whose concentration determines how elastic the hydrogel would be and how much it would swell. As the concentration of MBA is very low (0.010 g), the hydrogel swells greatly to the extent of 1340% (Fig. 11), as the structure is not compactly cross-linked, hence having elastic properties and absorbing plenty of water [28]. However, this less compactly cross-linked structure lacks robustness.

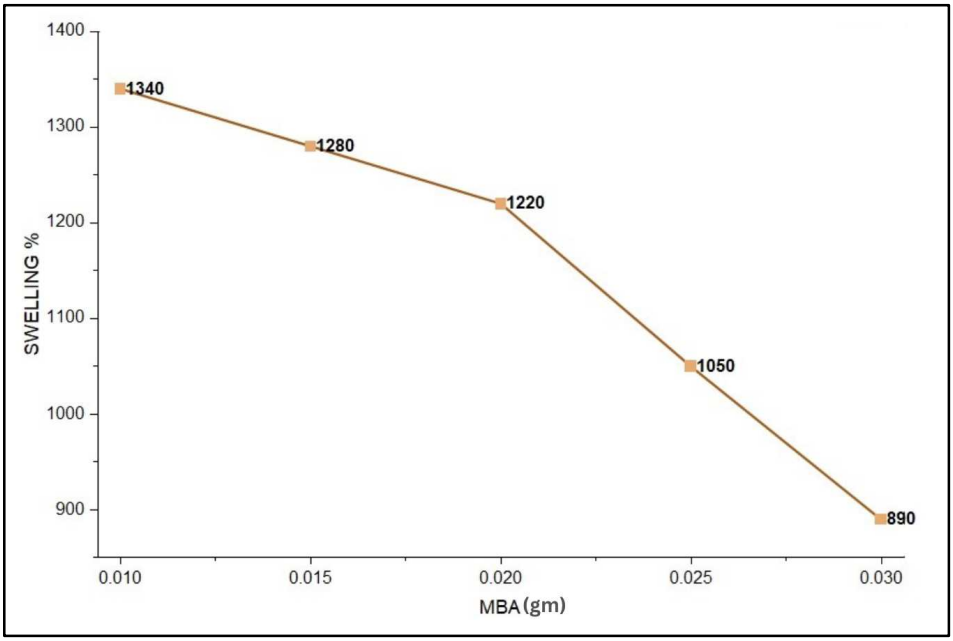


Fig. 11 Effect of MBA on the equilibrium swelling behavior of the CMTKG-GG-PAM hydrogel

As the concentration of MBA is increased to the optimum level (0.020 g), the swelling ability is also balanced to 1220%, as the structure is not only stable to retain its shape but also elastic to hold water [29]. As the concentration of MBA is increased to the higher side (0.025-0.030 g), the swelling ability reduces substantially to 1050% and 890% (Table 5), respectively, as the structure is compactly cross-linked and hence non- elastic, with the result that the space is pushed out where the water can enter [27].

TABLE 5 Effect of MBA on the equilibrium swelling behavior of the CMTKG-GG-PAM hydrogel.

Sample	**CMTKG**	**GG**	**AAm**	**MBA**	**KPS**	**Swelling percent**	**Gel Fraction**	**Porosity**
A16	0.5	0.5	3	0.01	0.045	1340	82	62.5
A17	0.5	0.5	3	0.015	0.045	1280	87	60

A18	**0.5**	**0.5**	**3**	**0.02**	**0.045**	**1220**	**91.5**	**58.2**
A19	0.5	0.5	3	0.025	0.045	1050	94	52.5
A20	0.5	0.5	3	0.03	0.045	890	96.5	48

Effect of KPS

The role of a radical initiator in free radical polymerization is played by potassium persulfate (KPS), thus determining the extent of Polymer chains formed and final network robustness of hydrogel formed. In a condition where concentration of KPS is lower (0.030 g), swelling is reduced to a lower extent of around 950% (Fig. 12) due to a lower number of radicals to facilitate complete polymerization [30]. This leads to lower polymer chains and a loosely formed network with reduced ability to retain water.

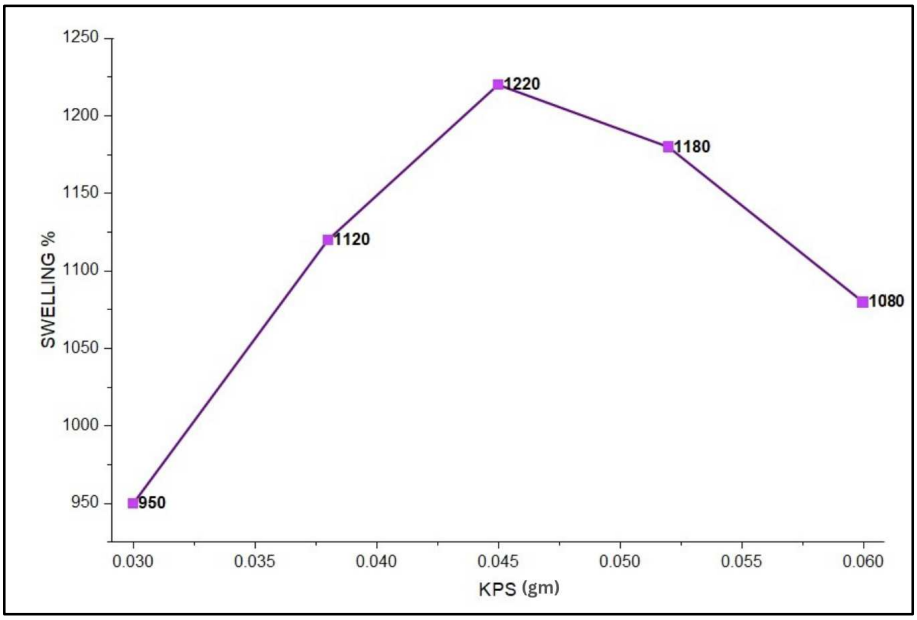


Fig. 12 Effect of KPS on the equilibrium swelling behavior of the CMTKG-GG-PAM hydrogel.

However, an optimum concentration of KPS (0.045 g) leads to an increase in swelling to a maximum of around 1220%, indicating an appropriate concentration of radicals in facilitating complete and efficient polymerization [31]. The final network formed would therefore be of appropriate chain size and cross-linked density to allow effective absorption of water. However, increasing KPS concentration (above 0.052-0.060 g) leads to a subsequent reduction in swelling to around 1180% and 1080%, respectively. An excess of KPS may therefore result in termination of reaction due to oligomers and over-cross-linking, thus inhibiting network expansion with reduced free volume of water [32].

TABLE 6 Effect of KPS on the equilibrium swelling behavior of the CMTKG-GG-PAM hydrogel.

Sample	**CMTKG**	**GG**	**AAm**	**MBA**	**KPS**	**Swelling percent**	**Gel Fraction**	**Porosity**

A21	0.5	0.5	3	0.02	0.030	950	84	50
A22	0.5	0.5	3	0.02	0.038	1120	88.5	54.8
A23	**0.5**	**0.5**	**3**	**0.02**	**0.045**	**1220**	**91.5**	**58.2**
A24	0.5	0.5	3	0.02	0.052	1180	93	57
A25	0.5	0.5	3	0.02	0.060	1080	94.5	53.5

Gel fraction

Effect of CMTKG

The gel fraction, the portion of the hydrogel that is cross linked and insoluble, increases with the rise in the amount of CMTKG until it reaches an optimal point at which the network is reinforced. When the amount of CMTKG is only 0.3 g (Fig. 13), the gel fraction is already at 85.0% meaning that there is not enough polymer backbone available for successful combination with the MBA, and some oligomers are still soluble or unreacted [33]. Then, at 0.5 g CMTKG, the gel fraction reaches an optimal point of 91.5% because the biopolymer component is rich enough in hydroxyl and carboxyl groups, which are used in cross linkages, thereby having a robust three-dimensional network [33].

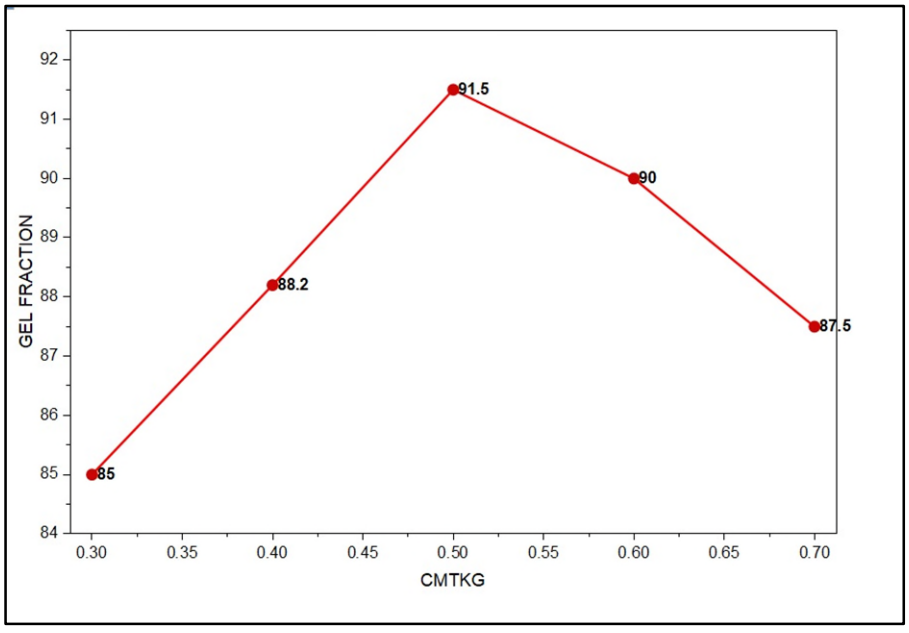


Fig. 13 Effect of CMTKG on the Gel Fraction of the CMTKG-GG-PAM hydrogel

As the amount of CMTKG is raised again beyond 0.6–0.7 g, the gel fraction slightly decreases to 90.0% and 87.5% because the excess amount is congested, which may have resulted in steric hindrance, reduced accessibility for the cross linkers, and may have resulted in more physical than chemical network formation.

Effect of GG

With low guar gum content-0.3 the gel fraction is 86.0%, because there is not enough strong polymer backbone, which has become necessary in order to be cross linked effectively with N,N'-methylenebisacrylamide (MBA), leaving more polymer chains soluble or unreacted [34]. At an optimum amount of 0.5 g (Fig. 14), the gel fraction was at its maximum, 91.5%, since guar gum provides adequate crosslinking sites to form a stable and well-integrated three-dimensional network [35].

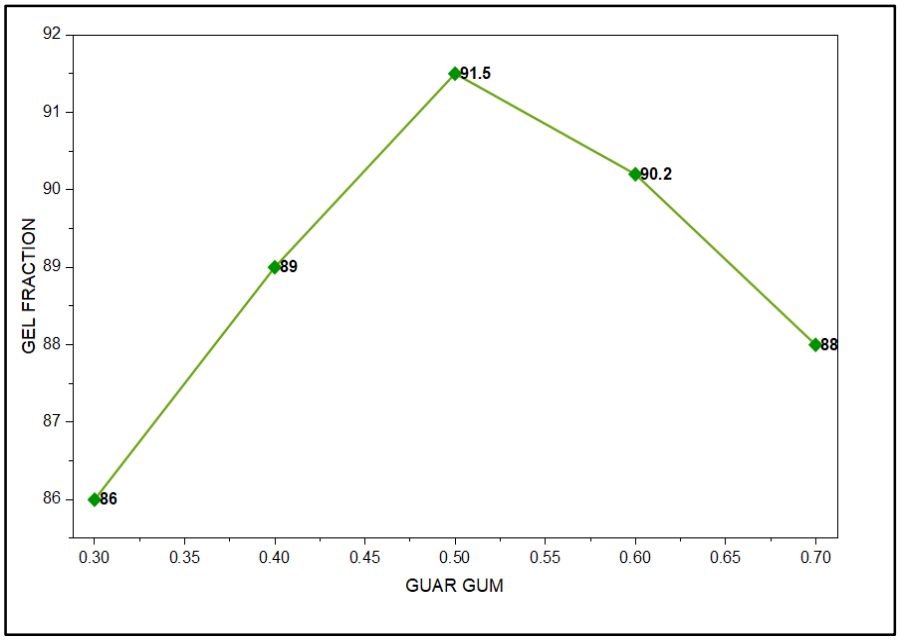


Fig. 14 Effect of GG on the Gel Fraction of the CMTKG-GG-PAM hydrogel

A further increase in guar gum within the range 0.6-0.7 g yields a small decline in the gel fraction to 90.2-88.0%. This might be ascribed to steric hindrance and crowding of the chains that may impede uniform crosslinking and allow physical entanglement to be favored over efficient chemical crosslinking, with a reduction in overall efficiency.

Effect of AAm

At a relatively low content of acrylamide of 2.0 g, the gel fraction decreases to 88.0% because of a lack of sufficient monomer to achieve a complete cross-linkable network structure. However, at a critical concentration of 3.0 g, according to optimization, the gel fraction increases to 91.5% (Fig. 15), indicating successful free radical polymerization and cross-linking by MBA (N,N'-Methylenebis-acrylamide) [36].

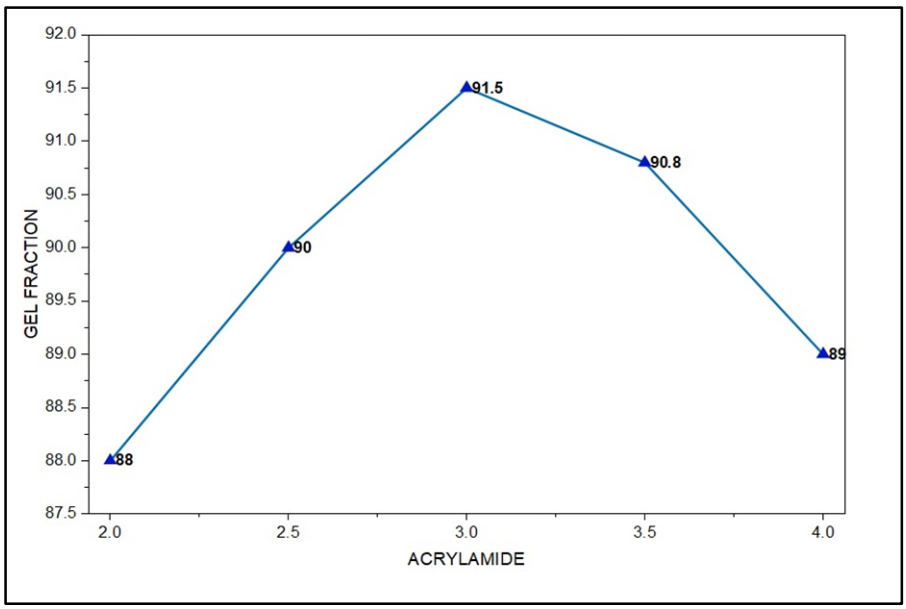


FIG. 15 Effect of Acrylamide on the Gel Fraction of the CMTKG-GG-PAM hydrogel

A tough, insoluble three-dimensional network has formed under these conditions. Increasing the content of acrylamide to a relatively higher value of 3.5-4.0 g leads to a progressive decrease in the gel fraction to values of 90.8-89.0%, respectively [37]. It may be attributed to the kinetic chain transfer or termination reaction, especially with relatively heavier monomer concentrations, resulting in a greater tendency for chain growth and lesser cross-linking efficacy.

Effect of MBA

With the lowest concentration (0.010 g) of MBA, the gel fraction is a remarkable 82.0%, indicating a lack of crosslinking and a significant presence of free polymer chains or unreacted oligomers in solution [38]. At the point of ideal concentration (0.020 g), the gel fraction significantly rises to 91.5% (Fig. 16), establishing an ideal crosslinking process whereby the polymer chains are immobilized in their three-dimensional structure as an insoluble network [39].

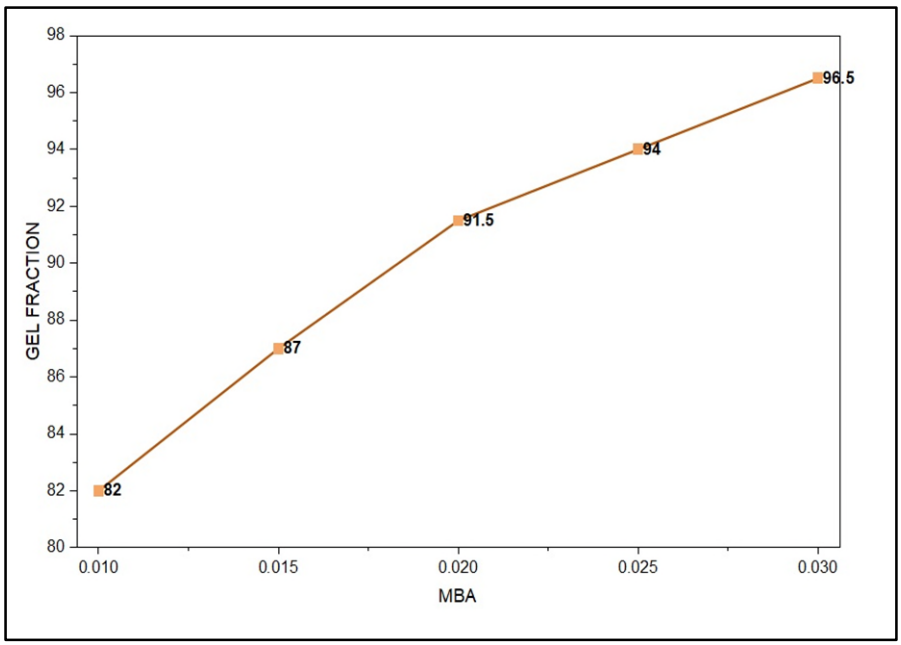


Fig. 16 Effect of MBA on the Gel Fraction of the CMTKG-GG-PAM hydrogel.

Further increasing the concentration with MBA (0.025-0.030 g) indicates a rise in the gel fraction to 94.0% and then to 96.5%, indicating a near-complete involvement of polymer chains within the cross linked structure. This indicates a concomitant decrease in the degree of swelling.

Effect of KPS

The amount of KPS used greatly affects how much stays cross linked and insoluble in the hydrogel, as it controls the degree of initiation and the extent of polymerization [40]. A low KPS amount of 0.030 g gives 84.0% (Fig. 17) for the gel fraction, meaning poor initiation occurs together with partial crosslinking; thus, a large part of the polymer chains and unreacted monomers remains soluble [41].

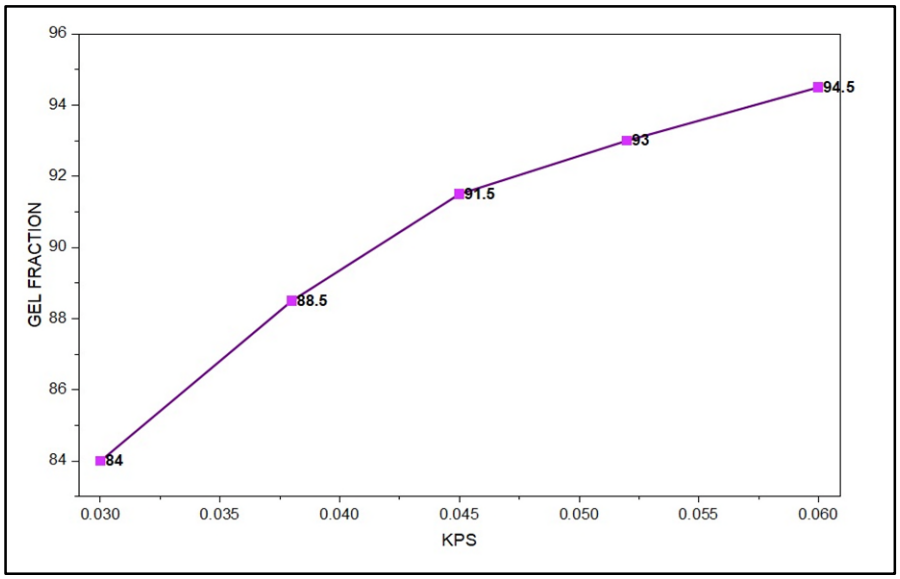


Fig. 17 Effect of KPS on the Gel Fraction of the CMTKG-GG-PAM hydrogel.

For the proper KPS amount of 0.045 g, the gel fraction is 91.5%; thus, the formation of radicals and the chain propagation are effective, and a strong crosslinking occurred, which therefore produced a solid three-dimensional network that was insoluble [42]. Further increasing KPS to 0.052–0.060 g results in even higher gel fractions: from 93.0% to 94.5%. Increasing KPS accelerates polymerization and crosslinking. However, higher gel fractions do not always lead to better performance, since too much compactness can impede swelling and reduce porosity [43].

Porosity

Effect of CMTKG

Porosity, which reflects the internal structure of voids, is strongly associated with CMTKG concentration because porosity influences the mesh structure and chain expansion. For low CMTKG content (0.3 g), the value of porosity significantly decreases to 50.5% because of the compact structure of the polymer [44]. Consequently, a less swollen mesh with reduced pores is attained. For the optimum CMTKG content (0.5 g), the value of porosity reaches a maximum of 58.2% (Fig. 18) because of sufficient ionic repulsion between the -COO^- ions that leads to the expansion of the polymer chains [45].

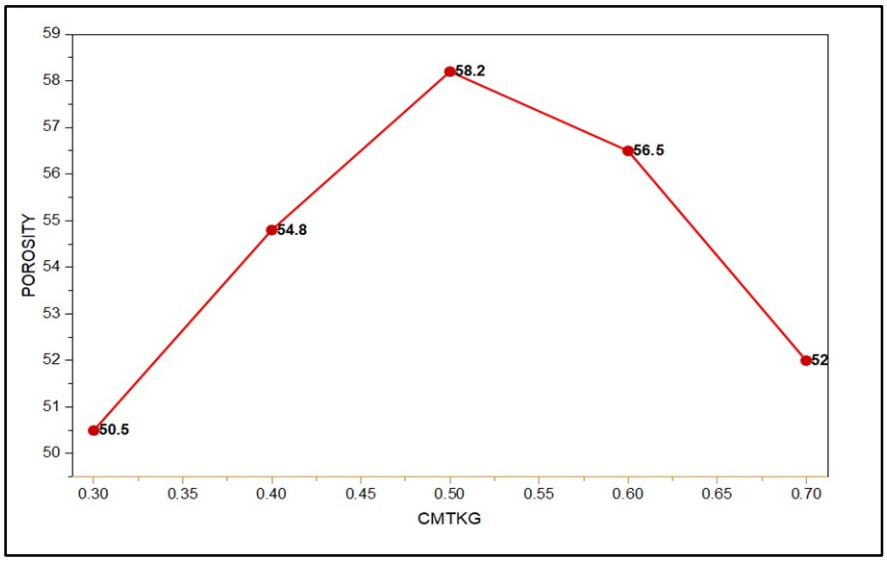


Fig. 18 Effect of CMTKG on the porosity of the CMTKG-GG-PAM hydrogel

Additionally, a well-defined mesh with micro- and macro-pores is created. For further increase in CMTKG content (0.6-0.7 g), a gradual decrease in the value of porosity up to 56.5-52.0% is attained [46]. The decrease might be because of the enhanced closure of the pores. A tightly packed mesh with a high degree of swelling might also occur.

Effect of GG

When we add a smaller amount of guar gum (0.3 g), the value of porosity decreases to 51.0% because, in this case, the polymer remains denser and compact, hence fewer and smaller pores are created. When we add the optimum amount of guar gum (0.5 g), the value of porosity increases to 58.2% (Fig. 19) due to its well-proportional mixture with the other factors, causing it to swell well to form a clear and well-interconnected pore structure [47].

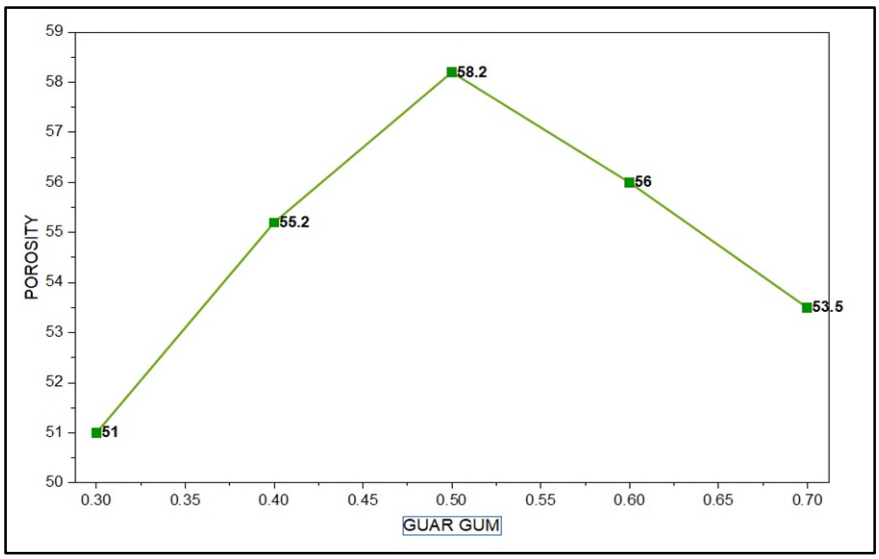


Fig. 19 Effect of GG on the porosity of the CMTKG-GG-PAM hydrogel

When we exceed this amount (0.6-0.7 g), the value of porosity reduces to the 56.0-53.5% range because, in this case, too much guar gum is added to make the polymer more dense, hence filling up the spaces of the pores and reducing their size, forming a more compact and hydrophilic network, which is still sponge-like [48].

Effect of AAm

With a low amount of acrylamide (2.0 g), the structure did not crosslink to become tough, so the value for porosity was lower at 52.0%, as the structure was voider with smaller pores. When it reaches the optimal point of 3.0 g, the porosity is at its highest, 58.2%, because the cross-linking is well-balanced [49]. The structure is highly uniform, with proper distances between chains, allowing for good swelling and the ability to form a network of micro- to macrospores (Fig. 20).

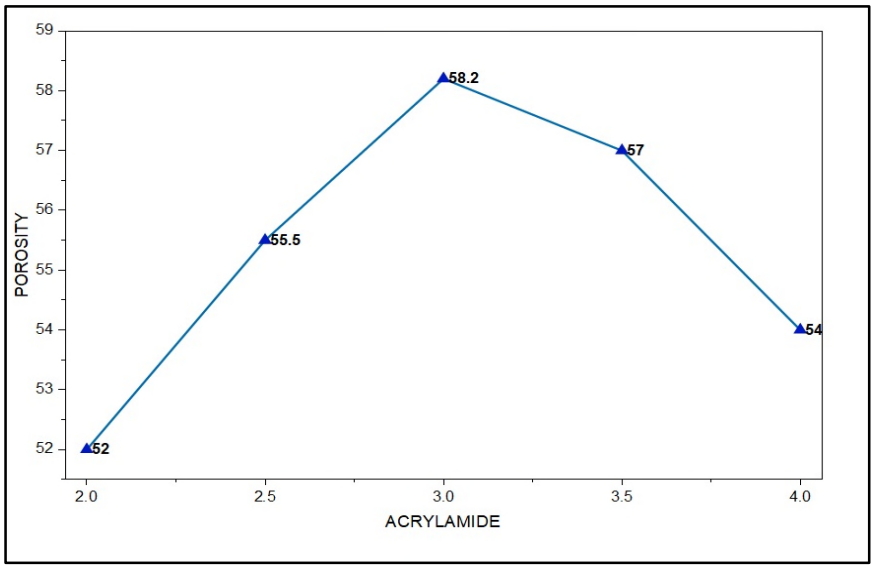


Fig. 20 Effect of Acrylamide on the porosity of the CMTKG-GG-PAM hydrogel

For greater amounts of acrylamide, ranging from 3.5 to 4.0 g, the porosity decreases to between 57.0% and 54.0% because the number of chains is already excessive to fill the spaces between them, making the structure more compact, even though the swelling capacity remains high.

Effect of MBA

At the lowest concentration of MBA (0.010g), porosity is highest at 62.5% (Fig. 21) because of the porous mesh structure that turns into huge pores. At the optimum concentration of MBA (0.020g), porosity is lower at 58.2% because of the higher crosslinking density that makes the pores less open while maintaining connectivity to allow fluid flow in the porous network structure [50].

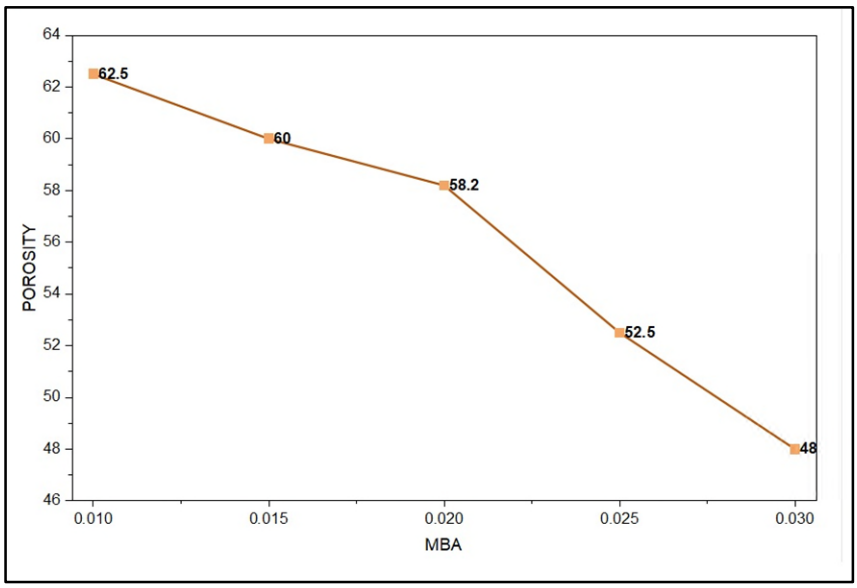


Fig. 21 Effect of MBA on the porosity of the CMTKG-GG-PAM hydrogel

At higher concentrations of 0.025-0.030g of MBA, porosity decreases significantly to 52.5% and 48%, respectively, because of the high crosslinking that leads to a dense structure with little room between the links to form pores that can allow the fast diffusion of fluid in the hydrogel structure.

Effect of KPS

Porosity, as a function of the internal pores of the hydrogel and how well they are interconnected, depends on the quantity of KPS, which affects the rate at which the polymerization procedure happens and how well the network forms [51]. A low quantity of KPS (0.030 g) results in reduced porosity to 50.0% (Fig. 22) because of incomplete polymerization, hence forming a network with poor, scattered interconnections and few pores.

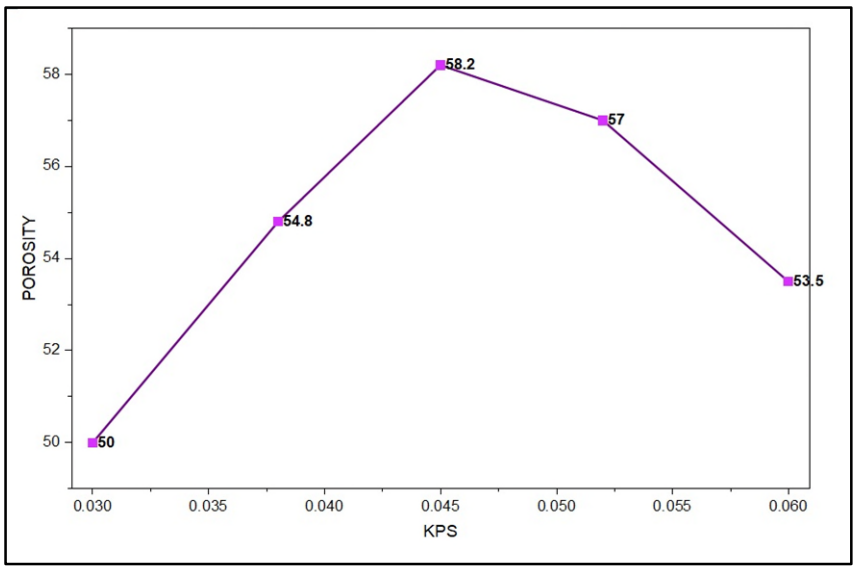


Fig. 22 Effect of KPS on the porosity of the CMTKG-GG-PAM hydrogel

When at the ideal concentration (0.045 g) of KPS, the highest porosity of 58.2% is achieved due to consistent and full polymerization, hence forming a well-regular network with well-defined and well-connected pores for enhanced fluid permeability and retention [17]. Whereas at a higher concentration of KPS (0.052-0.060 g), porosity decreases to 57.0% and 53.5%, respectively, because of accelerated polymerization due to increased radicals, hence creating a less regular network with higher cross-linking and smaller pores with low interconnectivity, hence affecting permeability and ability to swell [52].

Concentration-Dependent Sensing Study

The colorimetric response of the hydrogel film to different concentrations of heavy metals was studied. Using urine spiked with known concentrations of the three metals from our study (results not shown), we quantitatively analyzed the hydrogel film's colorimetric response by measuring both the color intensity and absorbance (using UV-VIS) at specific wavelengths [53]. As the concentration of each heavy metal increased from 0.1 ppm to 0.5 ppm (Fig. 23), there was a clear relationship between the increasing concentration of the heavy metal and the intensity of the color in the hydrogel films. The UV-VIS absorbance data confirmed this relationship, with each metal–DTZ complex demonstrating an increase in absorbance at characteristic wavelengths (for example, the linear increase in absorbance at 520 nm for the Pb^{2+}–DTZ complex; therefore, it demonstrates the potential of this system to detect low levels of heavy metals in urine/spiked urine).

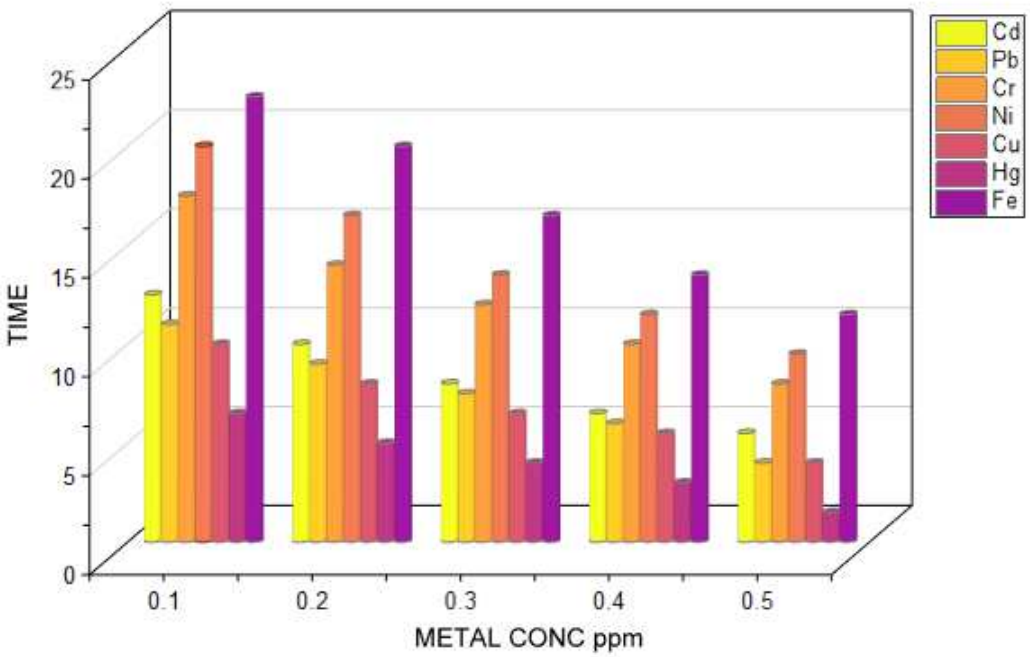


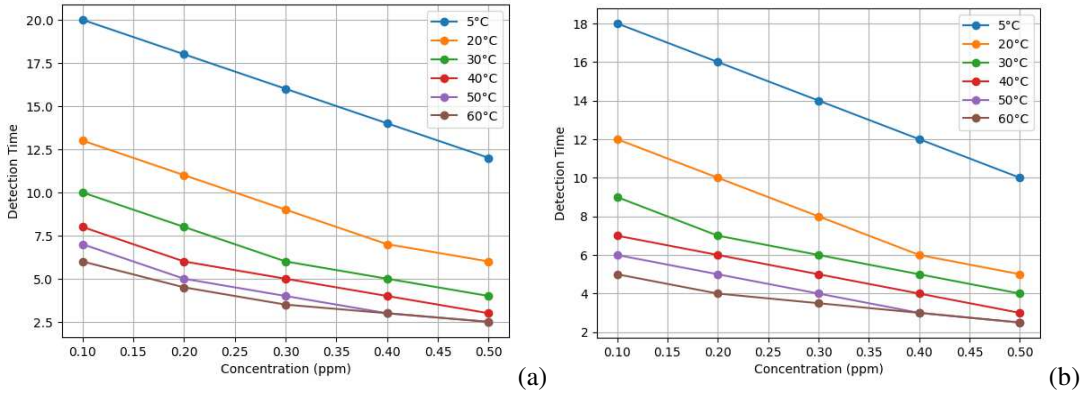
Fig. 23 Effect of metal ion concentration (ppm) on the response time of the DTZ-functionalized hydrogel sensor

The limit of visual detection of most of the metals was determined to be 0.1 ppm. This is important in light of the accepted limits for occupational exposure established by the relevant health organizations.

Temperature-Dependent Sensing Study

A temperature-dependent sensing performance study was performed within the range of 5-60 °C to assess the effect of different types of environment and physiology on the first hydrogel created that responds to colorimetric detection of drugs.

The film responded consistently over the temperature range of 20 °C to 40 °C, with maximum intensity and stability occurring at around 25- 37 °C. Response times were slightly delayed at lower temperatures (5-15 °C), while faster color development occurred at elevated (>50 °C) temperature, but less colour and more rapid partial desorption of DTZ occurred, suggesting that the hydrogel sensor was most reliable between standard room and body temperature, and therefore could be used as a point-of-care sensor without extreme thermal regulation (Fig. 24).



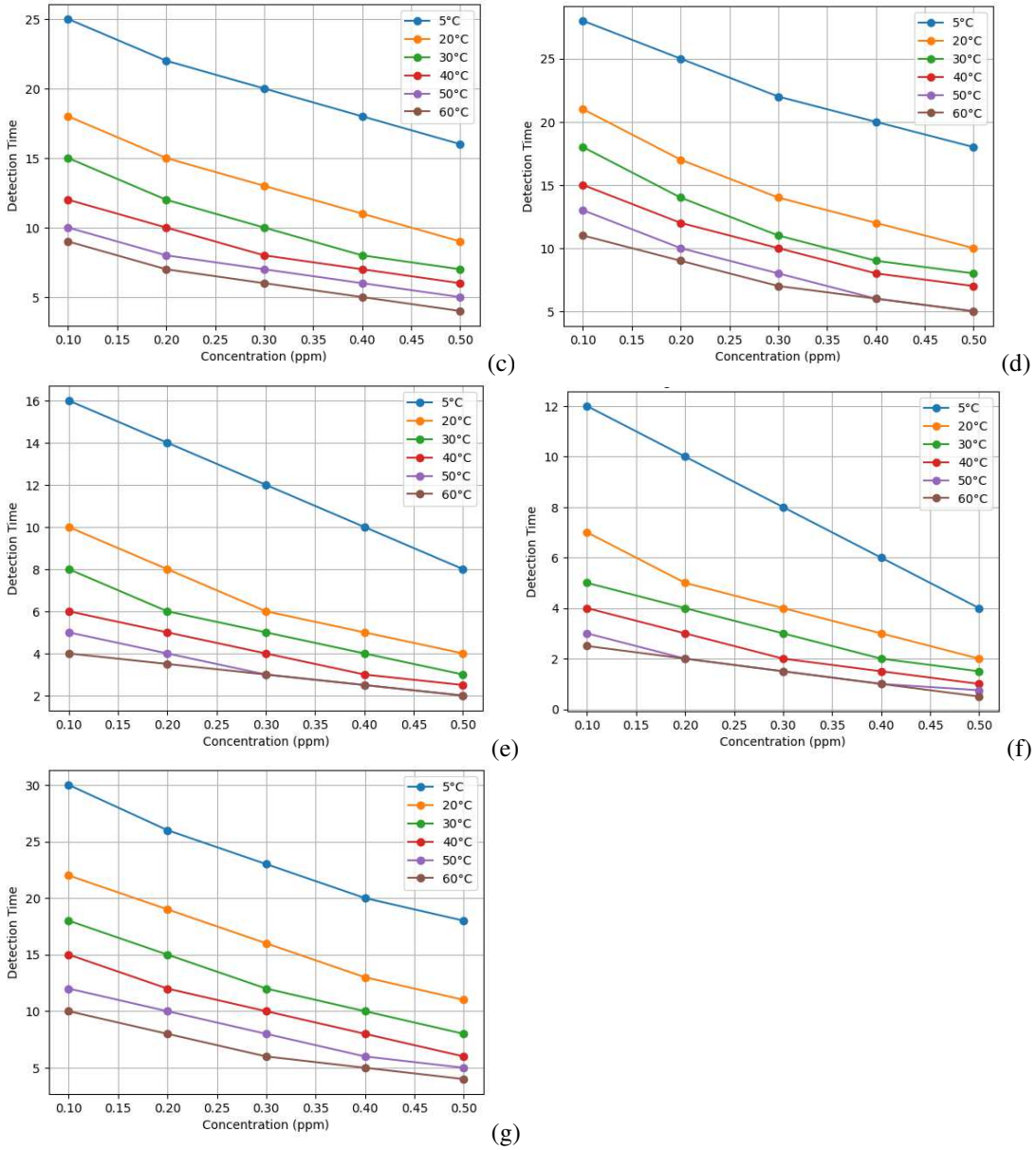


Fig. 24 Effect of Temperature on the response time (sec) of the DTZ-functionalized hydrogel sensor

Selectivity and Co-existing Ion Interference

The selectivity tests were performed with common urine electrolytes like Na^{+}, K^{+}, Ca^{2+}, Mg^{2+}, Cl^{-}, PO_4^{3-}, Fe^{3+}, and Zn^{2+}. The DTZ–hydrogel film showed excellent selectivity for the target heavy metals, and none of the color interference from the coexisting ions was evident at physiologically relevant concentrations. The cross-reactivity among target metals was minimal; however, simultaneous detection of multiple ions produces composite color shifts that could be deconvolute using spectral analysis. This is a selective behavior that indicates the utility of the film in complex biological matrices like urine.

Proposed Mechanism of Sensing

The colorimetric sensing mechanism of the DTZ-functionalized CMTKG/Guar Gum/Acrylamide hydrogel is under the synergistic control of chelation chemistry, hydrogel diffusion kinetics, and matrix-metal interaction. Dithizone

(DTZ), a well-known chelating agent, contains both thiol (−SH) and azo (−N=N−) functional groups which act as soft Lewis bases having high affinity for borderline and soft metal ions like Hg^{2+}, Cu^{2+}, Pb^{2+}, Cd^{2+}, among others (Fig. 25). In the event of exposure to metal-contaminated urine, metal ions diffuse through the hydrophilic and porous hydrogel network driven by swelling of the natural gum-acrylamide matrix.

Inside the hydrogel, the metal ions coordinate with DTZ through sulfur and nitrogen donor atoms to form stable, colored metal–dithizone complexes. This coordination causes a strong ligand-to-metal charge transfer (LMCT) that changes the electronic absorption profile of DTZ and yields distinct, metal-specific color transitions-from yellow for Cd^{2+} to violet for Hg^{2+}. The hydrogel acts not only as an immobilization scaffold but also as a means to enhance the local concentration of DTZ while prolonging its stability against photo degradation and leaching.

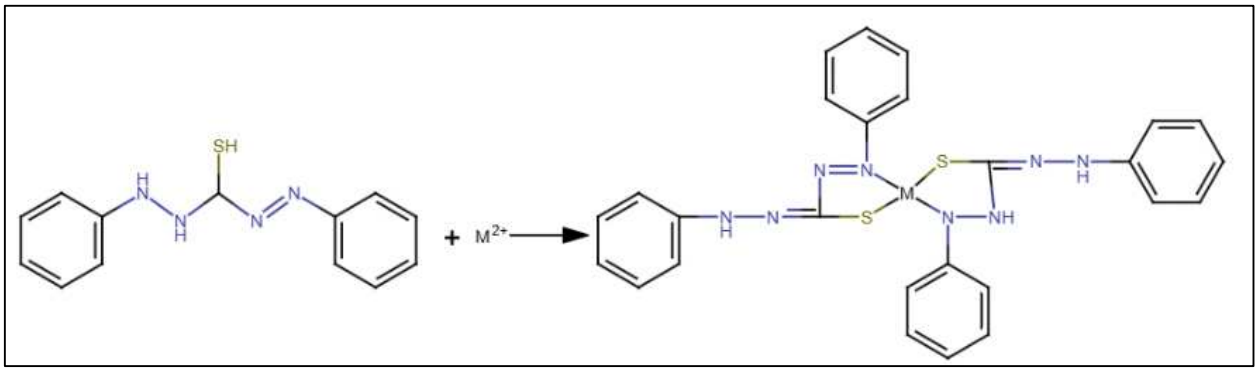


Fig. 25 Proposed mechanism of detection: formation of a Dithizone – Metal complex where M^{2+} (metal ion) is Pb^{2}, $^{+}Cd^{2+}$, Cu^{2+}, Ni^{2+}, Fe^{2+}, Cr^{2+}, Hg^{2+} ions

The continuous polysaccharide backbone in CMTKG and guar gum offers additional carboxylate and hydroxyl groups that could weakly bind the metal ions through electrostatic and coordination interactions, thus pre-concentrating metals around DTZ sites and thereby accelerating the kinetics of chelation. This dual-adsorption–chelation pathway also provided a good explanation for observed detection time reductions with increasing metal concentration and temperature. Both factors enhance the diffusion rate and complex formation kinetics [53]. Such temperature dependence can be related to greater mobility of both metal ions and polymer chains at higher temperatures, which allows faster penetration and binding, although too high a temperature may affect the stability of hydrogels and the retention of DTZ.

Characterization

FTIR (Fourier transform infrared)

Absorption bands located within the region of 3200-3400 cm^{-1}, which are due to the O-H and N-H stretching vibration modes, indicate the presence of functional hydroxyl and amine groups in the structure [54]. The peaks found in the vicinity of 2920 cm^{-1} relate to C-H stretching vibrations associated with aliphatic branches. The very intense peak at around 1600-1650 cm^{-1} corresponds to Amide I (C=O stretching) that is produced as a result of interactions from Carboxymethylation and crosslinking [55]. The C-O-C stretching vibration peaks located within the range of 1000-1150 cm^{-1} are due to the sugar backbone structure of polysaccharides.

The broad O-H band associated with the strong hydrogen bonding found in the guar gum spectrum at ~3300 cm^{-1} is a characteristic of polysaccharides [56]. The near 2925 cm^{-1} peak derives from the C-H stretching vibrations, while the peaks between ~1020-1100 cm^{-1} are characteristic of typical C-O and C-O-C polysaccharide structure stretching vibration modes, which serve as evidence to support the continued integrity of guar gum products in their formulations [57].

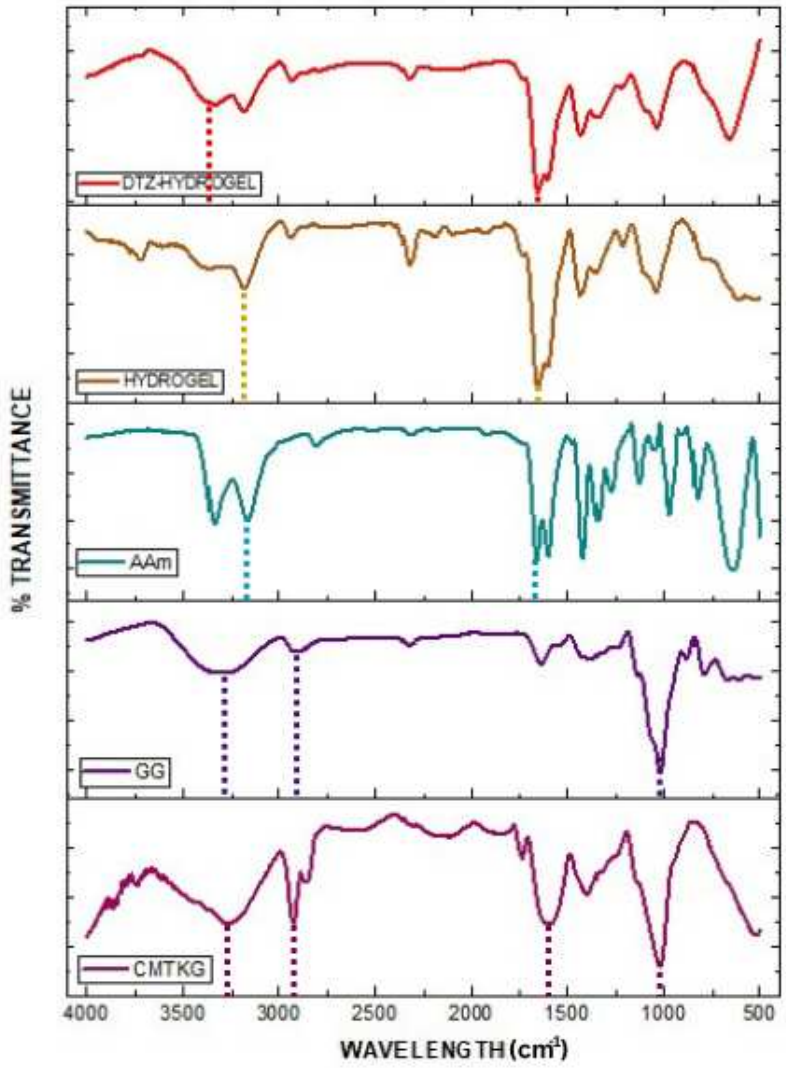


Fig. 26 FTIR spectra of (a) CMTKG-GG-PAM hydrogel incorporated with dithizone (b) CMTKG-GG-PAM hydrogel (c) Acrylamide (d) Guar Gum (e) CMTKG .

The acrylamide spectrum shows a strong absorption peak at about 1660 cm^{-1} for C=O stretching of the amide group and peaks around 3200–3400 cm^{-1} corresponding to N–H stretching vibrations (Fig. 26). Other bands close to 1450–1550 cm^{-1} also correspond to N–H bending and C–N stretching, confirming that the functional groups arise from acrylamide monomers [58].

In the spectrum of the combined hydrogel, significant peak position and intensity variations are present. A broadened, slightly lower wavenumber shifted O–H/N–H stretching band suggests increased hydrogen bonding interactions amongst guar gum, acrylamide, and CMTKG. An amide I peak at around 1650 cm^{-1} has been more clearly reflected, which further confirms graft copolymerization and network formation [59]. Reduced intensities of peaks due to the monomer also confirm the conversion of free acrylamide into the polymeric hydrogel structure [60].

The dithizone-loaded hydrogel (DTZ-HG) presents some additional spectral peaks over the blank hydrogel spectrum. The appearance of new peaks between 1400-1600 cm^{-1} relates to the presence of the dithizone molecules,

as shown by the presence of the A=C bond and the aromatic C=C bond stretches [61]. The slight shifts occurring within the amide and hydroxyl stretches relate to some interaction between the dithizone and the hydrogel main chain through hydrogen bonds as well as coordinate bonds. All the major peaks of the hydrogel backbone show that dithizone loading does not affect the backbone stability.

XRD (x ray Diffraction)

The CMTKG material has been characterized by having a broad diffraction peak centered in the 2θ value of 18°-22°, suggesting that this material has an amorphous structure with short-range ordering of molecules. It should be noted that this wide peak is characteristic of chemically modified polysaccharide-based materials [62].

This pattern for guar gum also possesses a wide peak in the range of 2θ ≈ 19–21° due to its semi-crystalline polymer nature (Fig. 27). The intensity of this peak for guar gum is less due to higher amounts of hydrogen bonds in its polysaccharide material [63].

The spectrum of acrylamide reveals well-defined peaks in its diffraction pattern, signifying its crystalline characteristics in monomer form. The high peak of acrylamide in its spectrum disappears in the spectrum of the hydrogel. This proves successful polymerization of acrylamide in forming a hydrogel network.

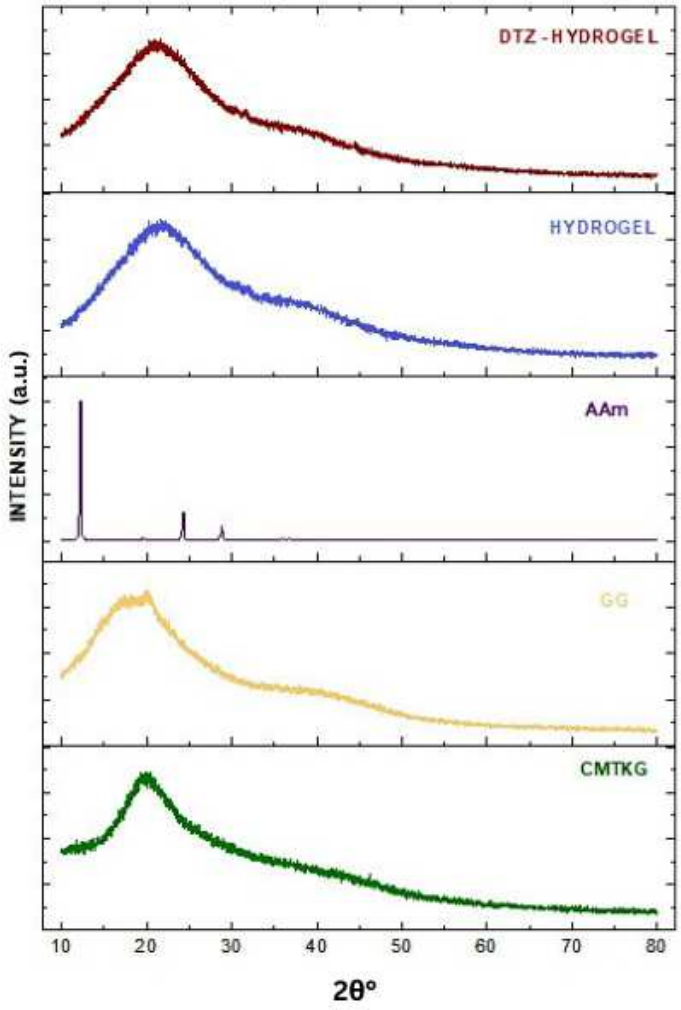
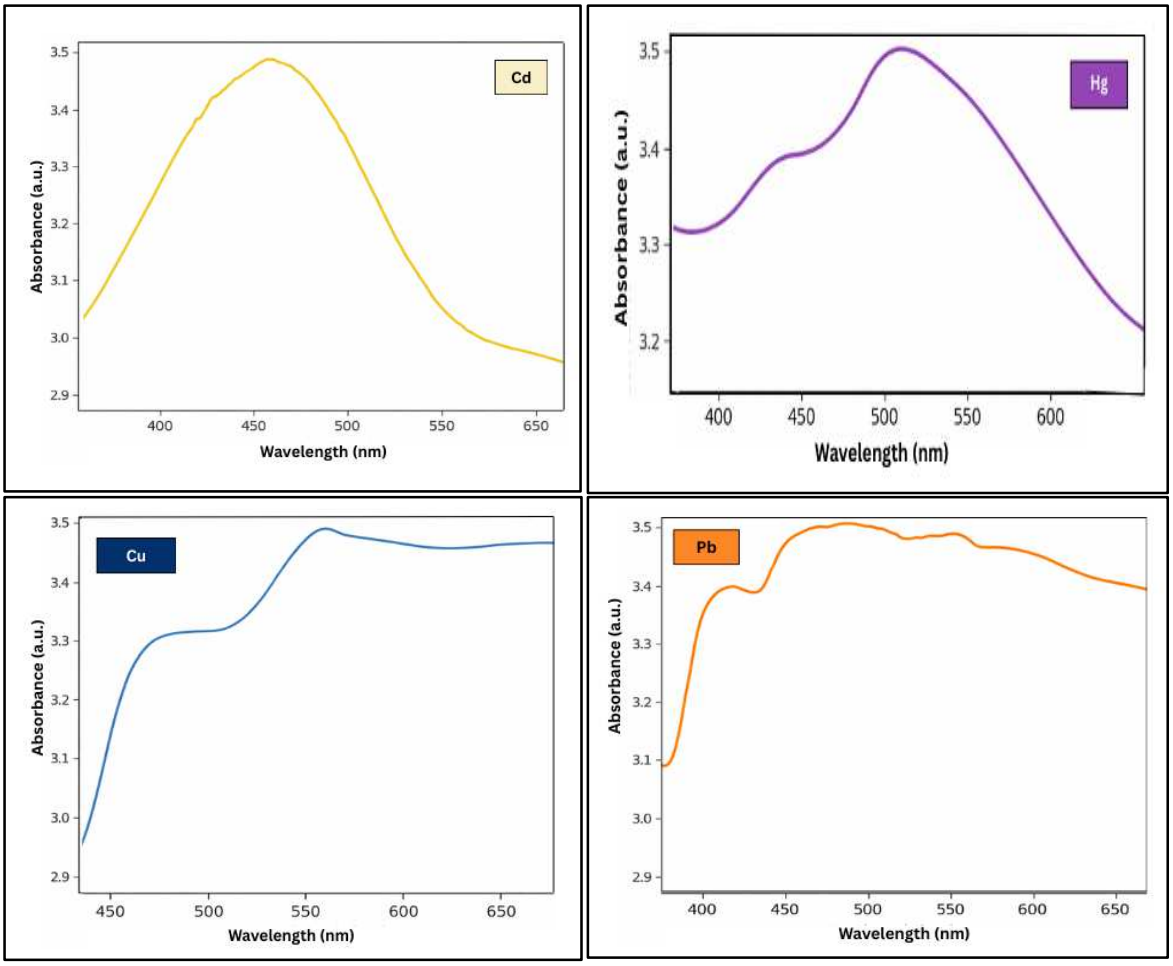


Fig. 27 XRD patterns of (a) CMTKG-GG-PAM hydrogel incorporated with dithizone (b) CMTKG-GG-PAM hydrogel (c) Acrylamide (d) Guar Gum (e) CMTKG

The combined hydrogel has a wide diffraction peak with less intensity. This supports that there was a randomly cross-linked polymeric network. A possible explanation could be that there are no sharp crystalline peaks in the combined hydrogel. This supports successful graft copolymerization onto a guar gum/CMTKG backbone [64].
The diffraction pattern of dithizone-loaded hydrogel (DTZ-HG) reveals a similar amorphous pattern, indicating slight peak broadening and variations in peak intensities, compared to that of blank hydrogel. The lack of prominent peaks due to free dithizone confirms that free dithizone appears to be well distributed throughout the hydrogel matrix in a more molecular form, as opposed to a distinct crystal form of free dithizone [65]. The effectiveness of dithizone immobilization in hydrogel, maintaining structural integrity of hydrogel, is thus proved.

UV (Ultraviolet-Visible spectroscopy)

The UV–Vis fingerprint of dithizone-loaded CMTKG/guar gum/acrylamide hydrogel indicates that the ligand is well immobilized and that metal-specific complexes form within the gel network. When free dithizone is present inside the hydrogel, it still exhibits characteristic visible-region bands between 380 and 480 nm from π→π* and n→π* transitions of the azo group –N=N– and thiocarbonyl group C=S (Fig. 28) [66]. The bands are slightly broader and more stable compared to those in the free solution, indicating strong physical entrapment and hydrogen bonding between dithizone and hydroxyl/amide groups of the CMTKG–guar gum–acrylamide matrix. This confirms that after loading, the sensing ligand remains chemically intact and optically active [67].



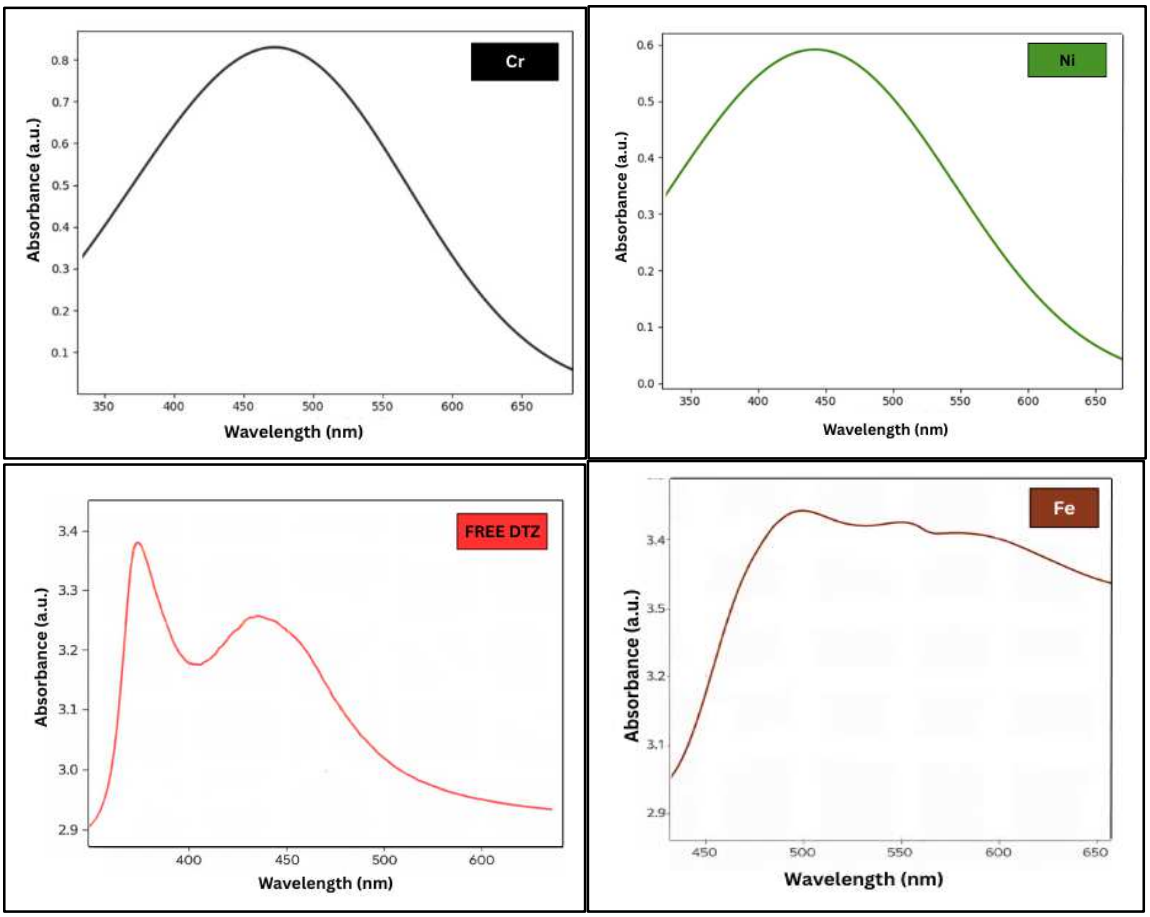


Fig. 28 UV spectra of (a) CMTKG-GG-PAM hydrogel incorporated with dithizone (b) CMTKG-GG-PAM hydrogel (c) Acrylamide (d) Guar Gum (e) CMTKG

The spectral changes of the hydrogel become specific, reproducible, and dependent on the kind of metal ion. In the presence of Hg^{2+}, well-pronounced bathochromic shifting occurred with a substantial absorbance increase at 500–550 nm. This confirmed the strong Hg–S bonding and thus inferred the formation of a stable complex between Hg with dithizone, consistent with the well-observed color change from orange to violet. Pb^{2+} also gave significant increases in absorbance and band broadening in the visible region, showing that strong chelation was possible through sulfur and nitrogen donors [68]. However, there was a partial shifting of the peak pattern because lead has a larger ionic radius and geometry. With Cd^{2+}, the smoother and better-defined band close to 450–480 nm is due to fair stability and less extended electronic delocalization of the complex, as compared to that of Hg^{2+} and Pb^{2+} [69]. In general, Cu^{2+} yielded a broader spectrum extending to higher wavelengths (about 520–580 nm), probably coming from the ligand-to-metal charge transfer combined with d–d transitions characteristic of Cu (II) complexes [70]. The Fe-dithizone complex shows a different profile, with a broadened band and more subtle intensity changes that suggest a different coordination environment, perhaps mixed Fe^{2+}/Fe^{3+} states and redox activity within the hydrogel. Ni^{2+} exhibits lower overall absorbance with a broad, featureless band, supporting weaker complexation and a more symmetric coordination sphere, consistent with the lower affinity of dithizone for Ni^{2+} [71]. Cr species, in turn, generate a broad visible-band pattern that can be ascribed to charge-transfer and d–d transitions; this reflects coordination with dithizone and the impact of variable chromium oxidation states.

SEM (Scanning Electron Microscopy)

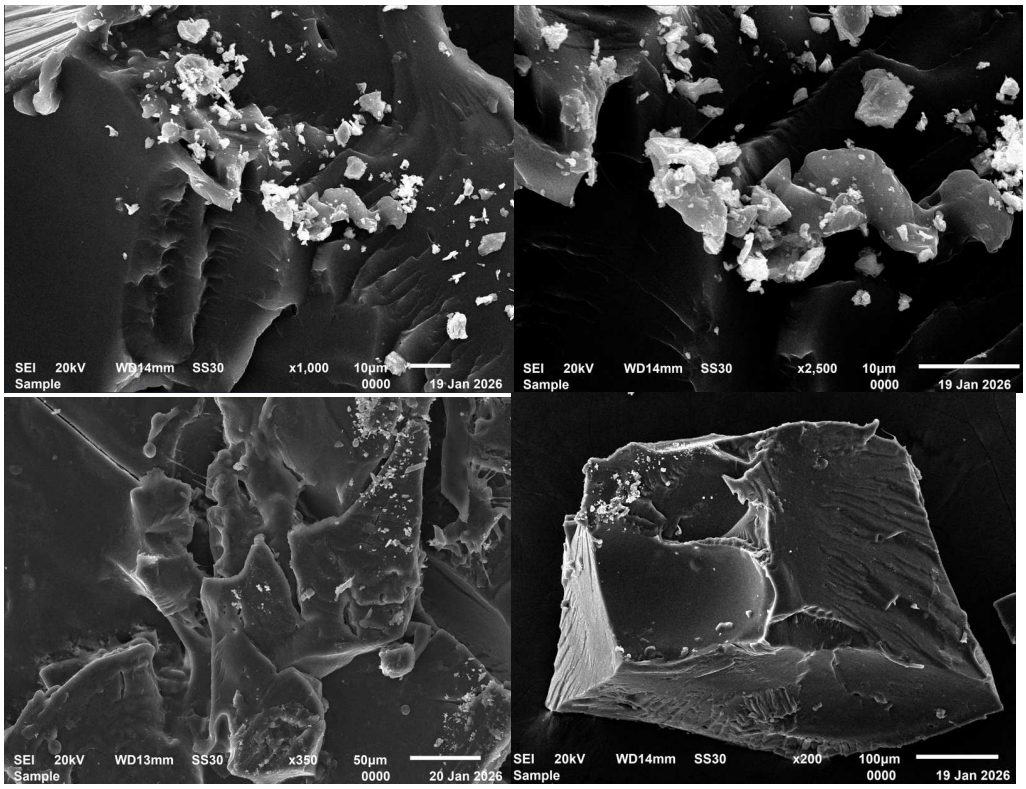


Fig. 29 SEM micrograph of CMTKG/Guar Gum/Acrylamide hydrogel

The SEM analysis of the CMTKG/Guar Gum/Acrylamide hydrogel reveals a complex, heterogeneous surface morphology characterized by a dense, cross-linked polymer matrix with irregular, flaky protrusions. At lower magnifications (x200 to x350), the hydrogel displays a relatively solid and brittle appearance with sharp fracture planes and "river-like" micro-channels, which are essential for facilitating water diffusion into the network (Fig. 29). As magnification increases to x2500, the surface shows significant roughness and the presence of small, integrated particulate clusters, indicating the successful grafting of the synthetic Acrylamide chains onto the natural polysaccharide backbones of the Tamarind and Guar gums. This lack of distinct phase separation suggests high compatibility between the components, while the folded, lamellar structures observed are likely a result of the dehydration process during sample preparation. Overall, the highly textured and porous topography provides a highly effective surface area, which is a favorable characteristic for applications in heavy metal adsorption, dye removal, or controlled drug delivery.

Conclusion

In summary, this study successfully developed a novel, dual-functional hydrogel composite based on Carboxymethyl Tamarind Kernel Gum (CMTKG), Guar Gum (GG), and Acrylamide (AAm) for the simultaneous detection and adsorption of heavy metals. By optimizing the concentrations of the biopolymers and cross-linking agents, the research identified a specific formulation that yields a robust, highly porous three-dimensional network with a maximum swelling capacity of 1220% at physiological pH. The successful immobilization of Dithizone (DTZ) within this matrix provided a sensitive colorimetric platform capable of producing distinct "naked-eye" color changes in response to toxic ions such as Lead, Cadmium, and Mercury at concentrations as low as 0.1–0.5 ppm.

The physicochemical analysis revealed that the hydrogel's performance is deeply rooted in the synergy between its natural and synthetic components, where the ionic character of CMTKG and the hydrophilicity of Guar Gum balance mechanical stability with high reactivity. With a gel fraction of 91.5% and optimized porosity, the material ensures both structural integrity and efficient mass transfer for metal sequestration. This innovation represents a

significant advancement in diagnostic technology, offering a low-cost, portable, and environmentally friendly alternative to expensive laboratory spectroscopy. Ultimately, the DTZ-functionalized hydrogel stands as a versatile tool for both point-of-care heavy metal screening in clinical urine samples and large-scale environmental remediation.

Acknowledgements The authors would like to thank Manav Rachna University (MRU) for providing infrastructure and instrumental facilities.

Author contribution S.J.: writing-original draft, writing-review & editing, investigation, software, conceptualization, methodology, visualization, formal analysis, validation. S.G.W. supervision, validation, and data curation. AS. : supervision, validation, and data curation All authors reviewed the manuscript.

Data availability No datasets were generated or analyzed during the current study.

Declarations

Ethics declarations

Competing interests The authors declare no competing interests.

Funding No funding was received for this work.

Consent to Participate and Consent to Publish declarations: not applicable.

References

1. Jagaba, A. H., Lawal, I. M., Birniwa, A. H., Affam, A. C., Usman, A. K., Soja, U. B., ... & Yaro, N. S. A. (2024). Sources of water contamination by heavy metals. In *Membrane technologies for heavy metal removal from water* (pp. 3-27). CRC Press.
2. Martinez-Morata, I., Sobel, M., Tellez-Plaza, M., Navas-Acien, A., Howe, C. G., & Sanchez, T. R. (2023). A state-of-the-science review on metal biomarkers. *Current environmental health reports*, *10*(3), 215-249.
3. Llaver, M., Oviedo, M. N., Quintas, P. Y., & Wuilloud, R. G. (2021). Analytical methods for the determination of heavy metals in water. In *Remediation of Heavy Metals* (pp. 1-50). Cham: Springer International Publishing.
4. Mousah, R. K., Zageer, D. S., & Kasar, K. A. (2025). Spectrometric Microfluidic Technique for Determination of Mercury (II) in Water Using Dithizone as Chromogenic Reagent. *Al-Nahrain Journal of Science*, *28*(2), 1-11.
5. Ivanova, V., Minkova, K., & Chakarov, K. (2026). Optimization Of The Extraction Conditions For The Hg^{2+}-Dithizone Complex In Chloroform And Its Determination By Uv-Vis Spectrophotometry. *Journal of Chemical Technology and Metallurgy*, *61*(1), 83-92.
6. Nanda, D., Behera, D., Pattnaik, S. S., & Behera, A. K. (2025). Advances in natural polymer-based hydrogels: Synthesis, applications, and future directions in biomedical and environmental fields. *Discover Polymers*, *2*(1), 6.
7. Sand A., N.-J. Shin, H.-G. Nam, and Y.-Je Kwark. "Effects of reaction parameters on water absorption of poly (itaconic acid) superabsorbent particles synthesized by inverse suspension polymerization." Fibers and Polymers 22, no. 4 (2021): 898-903. 10.1007/s12221-021-0459-2
8. Mahmood, T., Sarfraz, R. M., Mahmood, A., Salem-Bekhit, M. M., Ijaz, H., Zaman, M., ... & Benguerba, Y. (2024). Preparation, in vitro characterization, and evaluation of polymeric pH-responsive hydrogels for controlled drug release. *ACS omega*, *9*(9), 10498-10516.
9. Lubis, N., Gea, S., Tamrin, T., Tarigan, J. B., Piliang, A. F. R., & Goei, R. (2025, November). Characterization and evaluation of a cellulose-based hydrogel prepared from oil palm empty fruit bunches and crosslinked with citric acid. In *AIP Conference Proceedings* (Vol. 3195, No. 1, p. 040001). AIP Publishing LLC.

10. Warkar, S. G., & Kumar, A. (2019). Synthesis and assessment of carboxymethyl tamarind kernel gum based novel superabsorbent hydrogels for agricultural applications. *Polymer*, *182*, 121823.
11. Safari, J. B., Bapolisi, A. M., & Krause, R. W. (2021). Development of pH-sensitive chitosan-g-poly (acrylamide-co-acrylic acid) hydrogel for controlled drug delivery of tenofovir disoproxil fumarate. *Polymers*, *13*(20), 3571.
12. Mo, K., Lin, J., Wei, P., Mei, J., & Chang, C. (2021). Bioinspired gradient hydrogel actuators with rewritable patterns and programmable shape deformation. *Journal of Materials Chemistry C*, *9*(32), 10295-10302.
13. Zamani-Babgohari, F., Irannejad, A., Kalantari, M., & Khayati, G. R. (2025). Optimized Synthesis, Characterization and Swelling Study of Carboxymethyl Starch/Poly (Acrylamide-Co-Acrylic Acid) Hydrogel with Responsive Behavior. *Journal of Polymers and the Environment*, 1-24.
14. Ma, X., Zhou, X., Ding, J., Huang, B., Wang, P., Zhao, Y., ... & Xu, W. (2022). Hydrogels for underwater adhesion: adhesion mechanism, design strategies and applications. *Journal of Materials Chemistry A*, *10*(22), 11823-11853.
15. Lin, Q., Luo, D., Du, P., Zhang, W., Feng, H., Ma, X., & He, X. (2026). Electrostatic Interaction-Induced Clusteroluminescence of Polyelectrolyte with UCST Behavior. *Langmuir*.
16. Zhao, Y. H., Wang, G. K., & Jia, D. (2025). Tailoring Swelling Ratio of Smart Hydrogels by Utilizing Entropy-Driven Topologically Correlated Structures. *Small*, *21*(43), e08808.
17. Gayen, T. K., Ali, M. A., & Warkar, S. G. (2025). Carboxymethyl tamarind kernel gum bio-hydrogel for soil amendment and micronutrient release in sustainable agricultural technologies. *Polymer Bulletin*, *82*(17), 11857-11883.
18. Rani, I., Warkar, S. G., & Kumar, A. (2023). Removal of Cationic Crystal Violet dye using Zeolite-Embedded Carboxymethyl Tamarind Kernel Gum (CMTKG) based Hydrogel Adsorbents. *ChemistrySelect*, *8*(29), e202301434.
19. DAS, A., MUKHERJEE, K., & GIRI, T. (2024). Grafting Methacrylic Acid onto Carboxymethyl Tamarind Kernel Polysaccharide to Improve pH Sustained Release Responsive Hydrogel Matrix. *Indian Journal of Pharmaceutical Sciences*, *86*(5).
20. Moncho-Jordá, A., & Dzubiella, J. (2016). Swelling of ionic microgel particles in the presence of excluded-volume interactions: a density functional approach. *Physical Chemistry Chemical Physics*, *18*(7), 5372-5385.
21. Niu, Q., Xie, J., Li, J., An, Z., Xiao, H., Zhang, X., ... & Wang, Z. (2025). Superabsorbent polymers: Innovations in ecology, environmental, and diverse applications. *Materials*, *18*(4), 823.
22. El Sayed, M. M., & Shaalan, H. (2023). Swelling Kinetics of Acrylamide Grafted Polysaccharides Blend Hydrogel.
23. Shruthi, S. B., Rameshaiah, G. N., Roy, P., & Sailaja, R. R. N. (2026). Microwave-assisted grafting of dual-backbone guar gum/sodium alginate superabsorbent polymer: mechanistic insights into sustainable swelling kinetics and soil amendment potential. *Polymer Bulletin*, *83*(1), 30.
24. Dave, P. N., Bamaniya, S., & Singh, P. (2025). Rheo-Mechanical Insights into Gum Acacia-grafted-Poly (N, N-Dimethylacrylamide) Hydrogels Reinforced with Nickel–Cobalt Ferrite Nanoparticles. *Journal of Inorganic and Organometallic Polymers and Materials*, 1-16.
25. Aljarba, N. H., Afzal, M., Alkhateeb, M. A., & Alkahtani, S. (2025). Polyacrylamide functionalized polysaccharide based nanocomposite semi-interpenetrating polymeric network hydrogel for pH-responsive controlled release of a model neuroprotective drug. *RSC advances*, *15*(44), 37027-37038.
26. Zamani-Babgohari, F., Irannejad, A., Kalantari, M., & Khayati, G. R. (2025). Optimized Synthesis, Characterization and Swelling Study of Carboxymethyl Starch/Poly (Acrylamide-Co-Acrylic Acid) Hydrogel with Responsive Behavior. *Journal of Polymers and the Environment*, 1-24.
27. Bhatia, M., Zhang, S., & Ge, T. (2025). Effects of Topological Constraints on Equilibrium Swelling of Polymer Gels. *ACS Polymers Au*.

28. Kim, S. U., Kim, Y. J., & Lee, T. H. (2025). Polysaccharide Hydrogel-Assisted Biosensing Platforms for Point-of-Care Use. *Biosensors*, *15*(1), 13.
29. Luo, Y., Pauer, W., & Luinstra, G. A. (2025). Nonlinear viscoelasticity of and structural modulation in guar gum-enhanced triple-network hydrogels. *Polymers*, *17*(5), 597.
30. Aljeboree, A. M., Jasim, K. K., & Sabah, N. A. (2025). High-capacity dye adsorption by low-cost combo hydrogel: kinetic, thermodynamic, and regeneration study. *Journal of Inorganic and Organometallic Polymers and Materials*, *35*(10), 8350-8373.
31. Wang, Y., Yuan, W., Liang, Q., Lv, H., Liu, X., Zhao, L., & Wu, J. (2024). Fast Gelation and Mechanical Reinforcement of Tetrahydroxydiboron-Induced Free Radical Polymerized Hydrogels under Harsh Conditions. *Macromolecules*, *57*(21), 9965-9976.
32. Jayanudin, J., Lestari, R. S., Barleany, D. R., Pitaloka, A. B., Yulvianti, M., Kanani, N., ... & Rahmayetty, R. Ion-Responsive Chitosan-Graft-Poly (Acrylic Acid) Hydrogels Via Saponification: Structure, Swelling Kinetics, and Water Retention. *Swelling Kinetics, and Water Retention*.
33. Sharma, A., & Sand, A. (2025). Synthesis and application of carboxymethylated tamarind kernel gum (Fe-loaded) based superabsorbent hydrogels to investigate the effect on marigold plant growth. *Polymer Bulletin*, *82*(2), 397-422.
34. Pal, I., Chopra, L., Ganesan, S., Sharma, G. C., Bhowmik, A., & Santhosh, A. J. (2025). Guar Gum: Superabsorbent Hydrogels for Dye Remediation. *Polymers for Advanced Technologies*, *36*(1), e70080.
35. Xu, D., Zhao, Z., Ma, F., Xiong, J., Shi, H., Sun, X., ... & Lin, B. (2026). Design of polymer boron crosslinking agents based on scale effects and study of the crosslinking mechanism of guar gum at ultra-low concentrations. *International Journal of Biological Macromolecules*, 150086.
36. Nayak, A. K., & Pal, D. (2017). Functionalization of tamarind gum for drug delivery. *Functional biopolymers*, 25-56.
37. Batara, B., Steven, S., Mulyana, M., Saputra, A. S., Hutahaean, A. C., Yemensia, E. V., ... & Graha, H. P. R. (2025). Recent advances, applications, and challenges in superabsorbent polymers to support water sustainability. *Journal of Applied Polymer Science*, *142*(11), e56588.
38. Wei, Z., Liu, J., Zhang, J., Yang, L., Zhang, L., Wang, J., & Fan, H. (2024). The thermal stability mechanism of MBA-crosslinked PPGs: Insights from macroscopic phenomena to chemical reactions. *Polymer*, *309*, 127460.
39. Bhuyan, M. M., & Jeong, J. H. (2025). Preparation of Hydrogel by Crosslinking and Multi-Dimensional Applications. *Gels*, *11*(11), 896.
40. Lee, S. C., Gillispie, G., Prim, P., & Lee, S. J. (2020). Physical and chemical factors influencing the printability of hydrogel-based extrusion bioinks. *Chemical reviews*, *120*(19), 10834-10886.
41. Dastnaei, P. G. (2025). Hydrogels Synthesis through Various Polymerization Methods and Their Potential on Biomedical and Industrial Applications. *Prog. Chem. Biochem. Res*, *8*(4), 355-369.
42. Rodriguez-Gomez, P., Vega-Chacón, J., López, R., Florida, N., de Liss Meza Lopez, F., Sotomayor, M. D., & Picasso, G. (2025). Development of a New Ion-Imprinted Polymer (IIP) Using Dithizone as a Binding Agent for the Removal of Pb^{2+} From Real River Water Samples. *Polymer Engineering & Science*, *65*(10), 5348-5363.
43. Ahmed, M. S., Islam, M., Hasan, M. K., & Nam, K. W. (2024). A comprehensive review of radiation-induced hydrogels: synthesis, properties, and multidimensional applications. *Gels*, *10*(6), 381.
44. Sharma, A., & Sand, A. (2025). Tamarind Kernel Gum based superabsorbent polymer composite preparation and investigation of properties. *Journal of Polymer Research*, *32*(11), 1-19.
45. Fu, J., Yap, J. X., Leo, C. P., Chang, C. K., & Show, P. L. (2024). Polysaccharide hydrogels for controlling the nutrient release. *Separation & Purification Reviews*, *53*(3), 276-288.
46. Gayen, T. K., Ali, M. A., & Warkar, S. G. (2025). Cellulose microfibers-embedded carboxymethyl tamarind kernel gum hydrogels as soil conditioners and plant nutrients carriers. *ACS Agricultural Science & Technology*, *5*(6), 1132-1144.

47. Nandal, K., Vaid, V., Saini, P., Sharma, R. K., Joshi, V., Jindal, R., & Mittal, H. (2025). Synthesis and characterization of κ-carrageenan and guar gum-based hydrogels for controlled release fertilizers: Optimization, release kinetics, and agricultural impact. *Industrial Crops and Products*, *225*, 120587.
48. Díaz-Carrasco, F., De-Paz, M. V., Katavić, M., García-Pulido, E., Santos-Medina, Á., Muíña-Ramil, L., ... & Benito, E. (2025). Engineering Robust, Porous Guar Gum Hydrogels by One-Step Mild Synthesis: Impact of Porogen Choice on Rheology and Sustained Gastroretentive Amoxicillin Delivery. *Gels*, *11*(10), 785.
49. Sand, A., & Vyas, A. (2020). Superabsorbent polymer based on guar gum-graft-acrylamide: synthesis and characterization. *Journal of Polymer Research*, *27*(2), 43.
50. Yadav, M., Sand, A., & Behari, K. (2012). Synthesis and properties of a water soluble graft (chitosan-g-2-acrylamidoglycolic acid) copolymer. *International Journal of Biological Macromolecules*, *50*(5), 1306-1314.
51. Sand, A., Shin, N. J., Nam, H. G., & Kwark, Y. J. (2021). Effects of reaction parameters on water absorption of poly (itaconic acid) superabsorbent particles synthesized by inverse suspension polymerization. *Fibers and Polymers*, *22*(4), 898-903.
52. Shao, M., Gu, F., Fu, L., & Yue, X. (2022). Delayed Gelation Kinetics of In-Situ Polymerized Gel Based on the Mechanism of Living/Controlled Radical Polymerization. *ChemistrySelect*, *7*(18), e202104582.
53. Ma, J., Zheng, J., & Chen, J. (2025). Critical Mechanistic Insight, Technological Innovation Advances and Multi-Media Environmental Application of Colorimetry Toward Heavy Metal Detection. *Critical Reviews in Analytical Chemistry*, 1-33.
54. Meena, P., Singh, P., & Warkar, S. G. (2023). Development and assessment of carboxymethyl tamarind kernel gum-based pH-responsive hydrogel for release of diclofenac sodium. *European Polymer Journal*, *197*, 112340.
55. Gieroba, B., Kalisz, G., Krysa, M., Khalavka, M., & Przekora, A. (2023). Application of vibrational spectroscopic techniques in the study of the natural polysaccharides and their cross-linking process. *International journal of molecular sciences*, *24*(3), 2630.
56. Shiam, M. A. H., Islam, M. S., Ahmad, I., & Haque, S. S. (2025). A review of plant-derived gums and mucilages: Structural chemistry, film forming properties and application. *Journal of Plastic Film & Sheeting*, *41*(2), 195-237.
57. Zahid, M. U. (2026). Functional Prominence of Natural Gum-Based Crosslinked Hydrogels for Wound Healing and Dye Degradation Applications. *Journal of Applied Polymer Science*, *143*(5), e58154.
58. Sand, A., & Kwark, Y. J. (2017). Modification of guar gum through grafting of acrylamide with potassium bromate/thiourea redox initiating system. *Fibers and Polymers*, *18*(4), 675-681.
59. Derkach, S. R., Voron'ko, N. G., & Kuchina, Y. A. (2022). Intermolecular interactions in the formation of polysaccharide-gelatin complexes: a spectroscopic study. *Polymers*, *14*(14), 2777.
60. Rando, G., Scalone, E., Sfameni, S., & Plutino, M. R. (2024). Functional bio-based polymeric hydrogels for wastewater treatment: from remediation to sensing applications. *Gels*, *10*(8), 498.
61. Dewi, I. R., Rujiralai, T., Putson, C., & Cheewasedtham, W. (2023). A novel double metal-dithizone functionalized polyurethane electrospun nanofiber and film for colorimetric determination of hexavalent chromium. *RSC advances*, *13*(5), 2852-2859.
62. Kumari, S., Rustagi, B., Meena, P., & Warkar, S. G. (2025). Carboxymethyl tamarind kernel gum-based superabsorbent hydrogel for release of copper micronutrient. *International Journal of Biological Macromolecules*, 146010.
63. Ashames, A., Ullah, K., Al-Tabakha, M., Khan, S. A., Hassan, N., Mannan, A., ... & Murtaza, G. (2022). Development, characterization and In-vitro evaluation of guar gum based new polymeric matrices for controlled delivery using metformin HCl as model drug. *PLoS One*, *17*(7), e0271623.
64. Li, N., Fan, Y., Dong, X., Ma, X., Chen, R., Chang, M., & Xu, G. (2025). Synthesis and characterization of a guar gum-based flocculant and its flocculation-dewatering mechanism in coal mine wastewater. *International Journal of Biological Macromolecules*, *308*, 142438.

65. Golmohammadi, G., Joolaei Ahranjani, P., Sereshti, H., Dehghan, K., Sadatfaraji, H., Karami, S., & Rashidi Nodeh, H. (2025). Trace isolation and photometric determination of cadmium ions in water using thermally reduced graphene-modified hybrid sol-gel composite. *Separation Science and Technology*, *60*(11), 1421-1435.
66. Sedghi, R., Heidari, B., Javadi, H., & Sayyari, N. (2022). Design and synthesis of colorimetric sensor based on dithizone@ TiO2/poly (tert-butyl acrylate-acrylic acid) nanocomposite for fast visual detection of mercury, lead and cadmium ions in aqueous media. *Environmental Nanotechnology, Monitoring & Management*, *18*, 100670.
67. Carrizo, B. G., Fiorentini, E. F., Wuilloud, R. G., & Escudero, L. B. (2024). Dithizone functionalized carbon nanofibers as novel nanomaterial for microextraction and determination of mercury in non-alcoholic beverages. *Microchemical Journal*, *204*, 111134.
68. Ntoi, L. L., Buitendach, B. E., & von Eschwege, K. G. (2017). Seven chromisms associated with dithizone. *The Journal of Physical Chemistry A*, *121*(48), 9243-9251.
69. Asweisi, A., Algheryani, K., & Hussein, R. (2022, June). Separation of Cadmium from Aqueous Solutions by Cloud Point Extraction Using Different Nonionic Surfactants. In *The 3rd conf. on the environmental sciences, Misrata, Libya* (pp. 5-6).
70. Ramdass, A., Sathish, V., Babu, E., Velayudham, M., Thanasekaran, P., & Rajagopal, S. (2017). Recent developments on optical and electrochemical sensing of copper (II) ion based on transition metal complexes. *Coordination Chemistry Reviews*, *343*, 278-307.
71. Yumin, L., Yonglong, L., An, G., Zheyu, S., Liang, C., & Aiguo, W. (2013). Colorimetric Response of Dithizone Product and Hexadecyl Trimethyl Ammonium Bromide Modified Gold Nanoparticle Dispersion to 10 Types of Heavy Metal Ions: Understanding the Involved Molecules from Experiment to Simulation.
72. Jiang, D., Zheng, M., Ma, X., Zhang, Y., Jiang, S., Li, J., ... & Li, L. (2023). Rhodamine-anchored polyacrylamide hydrogel for fluorescent naked-eye sensing of Fe3+. *Molecules*, *28*(18), 6572.
73. Hamza, M. F., Hamad, N. A., Hamad, D. M., Khalafalla, M. S., Abdel-Rahman, A. A. H., Zeid, I. F., ... & Salem, W. M. (2021). Synthesis of eco-friendly biopolymer, alginate-chitosan composite to adsorb the heavy metals, Cd (II) and Pb (II) from contaminated effluents. *Materials*, *14*(9), 2189.
74. Liu, S., Yang, Y., Shi, M., Shi, H., Mao, D., Mao, X., & Zhang, Y. (2022). Smartphone-based pure DNAzyme hydrogel platform for visible and portable colorimetric detection of cell-free DNA. *ACS sensors*, *7*(2), 658-665.
75. Sopianb, K. (2021). New graphene nanocomposites-based. *Handbook of Nanomaterials for Wastewater Treatment: Fundamentals and Scale up Issues*, 367.
76. Sahu, Y., Hashmi, A., Patel, R., Singh, A. K., Susan, M. A. B. H., & Carabineiro, S. A. (2022). Potential development of N-doped carbon dots and metal-oxide carbon dot composites for chemical and biosensing. *Nanomaterials*, *12*(19), 3434.